METABOLISM

HIF-1α inhibitor PX-478 preserves pancreatic β cell function in diabetes

Erwin Ilegems[1]*, Galyna Bryzgalova[1], Jorge Correia[2], Burcak Yesildag[3], Edurne Berra[4], Jorge L. Ruas[2], Teresa S. Pereira[1,2]*†, Per-Olof Berggren[1,5,6,7]*†

During progression of type 2 diabetes, pancreatic β cells are subjected to sustained metabolic overload. We postulated that this state mediates a hypoxic phenotype driven by hypoxia-inducible factor–1α (HIF-1α) and that treatment with the HIF-1α inhibitor PX-478 would improve β cell function. Our studies showed that the HIF-1α protein was present in pancreatic β cells of diabetic mouse models. In mouse islets with high glucose metabolism, the emergence of intracellular Ca^{2+} oscillations at low glucose concentration and the abnormally high basal release of insulin were suppressed by treatment with the HIF-1α inhibitor PX-478, indicating improvement of β cell function. Treatment of db/db mice with PX-478 prevented the rise of glycemia and diabetes progression by maintenance of elevated plasma insulin concentration. In streptozotocin-induced diabetic mice, PX-478 improved the recovery of glucose homeostasis. Islets isolated from these mice showed hallmarks of improved β cell function including elevation of insulin content, increased expression of genes involved in β cell function and maturity, inhibition of dedifferentiation markers, and formation of mature insulin granules. In response to PX-478 treatment, human islet organoids chronically exposed to high glucose presented improved stimulation index of glucose-induced insulin secretion. These results suggest that the HIF-1α inhibitor PX-478 has the potential to act as an antidiabetic therapeutic agent that preserves β cell function under metabolic overload.

INTRODUCTION

The onset of obesity-linked type 2 diabetes is a consequence of insufficient insulin secretion to compensate for insulin resistance. At early stages, expansion of pancreatic β cell mass and enhanced pancreatic β cell function counteract insulin resistance to maintain normoglycemia. With progression of the disease, sustained metabolic overload will lead to β cell dysfunction. Seminal studies have shown that β cell function is already reduced to 50 to 80% of normal at the time of type 2 diabetes onset (*1*, *2*). Impaired β cell function at onset of type 2 diabetes is correlated with impaired glycemic control regardless of the specific therapeutic intervention applied (*3*–*5*). Therefore, preservation or recovery of β cell function is an important strategy in the treatment of type 2 diabetes.

Abnormally high concentrations of basal plasma insulin are observed in overweight and obese patients with and without type 2 diabetes (*6*, *7*). In diabetic patients, high basal insulin is associated with high fasting glucose. In contrast, nondiabetic obese patients presenting elevated basal insulin have normal fasting glucose and normal tolerance to glucose. In addition, studies with nonhuman primates showed that, in obese prediabetic animals, an increase in basal insulin precedes the rise of fasting glucose concentration (*8*, *9*). These observations suggest that increased basal insulin secretion can occur, independently of hyperglycemia, in response to metabolic overload. The molecular pathways driving an increase in basal insulin concentration have, however, not been fully uncovered. Previous studies suggest that mechanisms involving reduced plasma membrane cholesterol or resulting from glucotoxicity or lipotoxicity could lead to high basal insulin values (*10*, *11*).

Due to the long-standing realization that insulin production declines because of β cell dysfunction, therapeutic strategies to improve β cell function have focused on the amplification of β cell insulin secretion. These approaches, which all increase the workload for a dysfunctional β cell, may not be as successful as initially predicted (*12*, *13*). The use of sulfonylureas has been shown to accelerate β cell demise and dysfunction (*3*). In addition, studies with streptozotocin (STZ)–induced diabetic immunosuppressed mice transplanted with human islets suggest that therapy with glucagon-like peptide 1 (GLP-1) analogs might have deleterious long-term effects on β cell function (*14*). In this context, it has been proposed that therapeutic interventions aiming at protecting and preserving β cell function without amplification of insulin secretion might prove to be a more successful approach in the treatment of type 2 diabetes (*12*).

Because of the high energy demands of insulin secretion, pancreatic β cells consume large amounts of oxygen in mitochondrial respiration. The dependence of β cell function on oxygen availability has previously been explored in two studies showing that in vitro exposure of β cells to high glucose concentrations leads to a cellular hypoxic phenotype with activation of the hypoxia-inducible factor–1α (HIF-1α) (*15*, *16*). HIF-1α activates transcription of a large group of genes encoding proteins involved in angiogenesis (vascular endothelial growth factor), erythropoiesis (erythropoietin), and glucose metabolism (*17*). The main impact of HIF-1α on glucose metabolism is the switch of energy production from mitochondrial respiration to glycolysis. The HIF-1α gene is constitutively expressed, and changes in its mRNA abundance have no major impact on HIF-1α activity. Thus, regulation at the level of protein degradation by a mechanism mediated by O_2 availability is the major determinant of

[1]The Rolf Luft Research Center for Diabetes and Endocrinology, Karolinska Institutet, SE-171 76 Stockholm, Sweden. [2]Department of Physiology and Pharmacology, Molecular and Cellular Exercise Physiology, Karolinska Institutet, SE-171 77 Stockholm, Sweden. [3]InSphero AG, Wagistrasse 27a, 8952 Schlieren, Switzerland. [4]Centro de Investigación Cooperativa en Biociencias CIC bioGUNE, 48160 Derio, Spain. [5]Diabetes Research Institute, Miller School of Medicine, University of Miami, Miami, FL 33136, USA. [6]Lee Kong Chian School of Medicine, Nanyang Technological University, Novena Campus, 308232 Singapore, Singapore. [7]School of Biomedical Sciences, Ulster University, BT52 1SA Coleraine, Northern Ireland, UK.
*Corresponding author. Email: erwin.ilegems@ki.se (E.I.); teresa.pereira@ki.se (T.S.P.); per-olof.berggren@ki.se (P.-O.B.)
†These authors contributed equally to this work as senior authors.

HIF-1α activity. At normoxia, HIF-1α is ubiquitinated by the von Hippel–Lindau protein (pVHL) E3 ubiquitin ligase complex and degraded by the proteasome (*18*–*22*). Therefore, inactivation of the VHL gene results in an oxygen-independent stabilization of HIF-1α (*23*, *24*).

High glucose concentrations can stabilize HIF-1α in isolated islets, and HIF-1α target gene activation has a major impact on glucose metabolism (*15*, *16*). We now hypothesize that HIF-1α is stabilized in pancreatic β cells of diabetic mouse models, leading to β cell dysfunction and thereby contributing to obesity-linked type 2 diabetes. To address this hypothesis, we investigated the presence of the HIF-1α protein in diabetic mouse islets and the functional consequences of treating islets under metabolic overload using the HIF-1α inhibitor PX-478. The small-molecule PX-478 prevents HIF-1α deubiquitination and increases its proteasome-dependent degradation (*25*). We studied the impact of PX-478 treatment on islet function by assessing insulin secretion and intracellular Ca^{2+} handling in islets where high glucose metabolism was induced by the glucokinase (GCK) activator GKA50. In addition, we evaluated the relevance of the treatment with the inhibitor PX-478 for the phenotype of diabetic mouse models. We used the leptin receptor–deficient db/db mouse as a model of obesity-induced type 2 diabetes, as well as STZ-induced diabetic mice that display reduced functional β cell mass without impairment of insulin resistance, to further understand the metabolic mechanism of the PX-478 effect. Last, we assessed the impact of PX-478 on human β cell function by treating human islet organoids after long-term exposure to high glucose concentration and measuring insulin release.

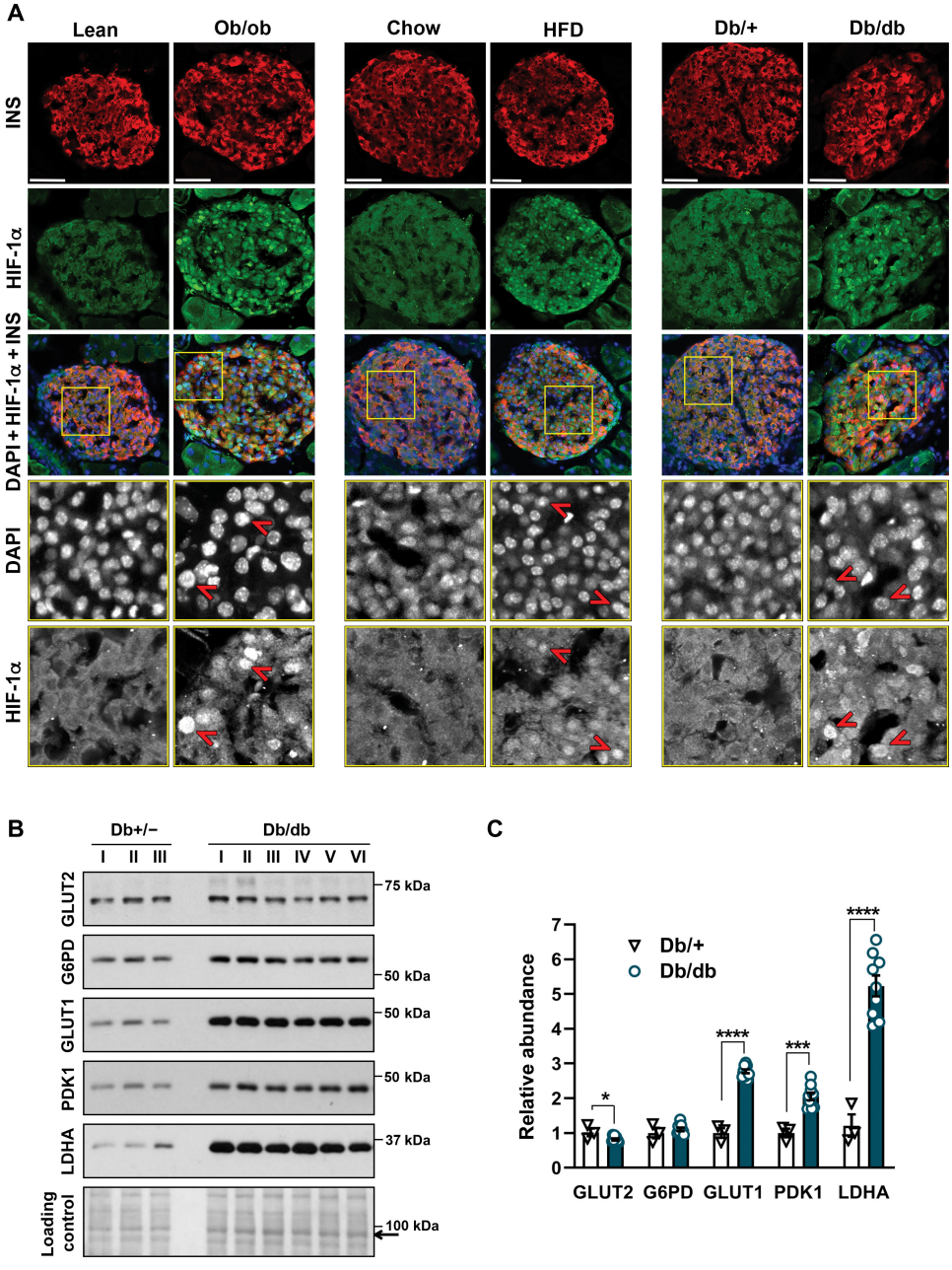

Fig. 1. The transcription factor HIF-1α is detected in β cells of diabetic mouse models. (**A**) Immunocytochemistry of frozen pancreas sections was performed using anti–HIF-1α or anti-insulin (INS) antibody. Nuclei visualization was done using 4′,6-diamidino-2-phenylindole (DAPI) staining. Yellow squares indicate the location of areas that were magnified. Red arrowheads indicate nuclei presenting positive staining for DAPI and HIF-1α in the magnified images. Images were acquired using confocal microscopy. (**B**) GLUT1, PDK1, and LDHA protein abundance in islets of 15-week-old db/db mice. Db/db ($n = 9$) or db/+ ($n = 3$) mouse islets were lysed, and Western blot analysis was performed. Ponceau staining was used as loading control. (**C**) Quantification of protein abundance presented in (B). The band indicated by an arrow in the Ponceau staining was used as internal control in the calculation of protein abundance. Scale bars, 50 μm. *$P < 0.05$, ***$P < 0.001$, and ****$P < 0.0001$ by two-tailed unpaired Student's *t* test.

RESULTS

HIF-1α protein is present in pancreatic β cells of diabetic mouse models

We have previously shown that pancreatic islets of db/db mice are positive for pimonidazole adducts, indicating that they are hypoxic (*26*, *27*). To further understand whether hypoxia mediates HIF-1α stabilization in β cells in diabetic mouse models, we performed immunocytochemistry using an anti–HIF-1α antibody. In contrast to islets of lean mice, we detected HIF-1α protein in the nuclear compartment of β cells within islets of ob/ob mice, mice fed a high-fat diet (HFD), and db/db mice (Fig. 1A). Furthermore, islets of db/db mice showed a robust increase in the abundance of several proteins encoded by classical HIF-1α target genes (*17*) such as glucose

transporter 1 (GLUT1), pyruvate dehydrogenase kinase 1 (PDK1), and lactate dehydrogenase 1 (LDHA) (Fig. 1, B and C), reinforcing the assumption that HIF-1α is active in diabetic mouse islets.

An acute increase in metabolic workload leads to cellular hypoxia in pancreatic islets of diabetic mouse models

Using pimonidazole as a hypoxia marker, we investigated whether an acute rise in metabolic workload in response to a glucose bolus could increase the formation of pimonidazole adducts in pancreatic islets of diabetic or prediabetic mouse models. Pancreatic islets of diabetic ob/ob or prediabetic HFD-fed mice presented higher amounts of pimonidazole adducts in response to glucose loading compared to nonobese controls (Fig. 2, A to C) or chow-fed mice (Fig. 2, D to F). These results indicate that, in mice with high glucose intolerance (Fig. 2, C and F), an acute increase in metabolic workload leads to a state of cellular hypoxia.

Increasing glucose metabolism in isolated mouse islets through GCK activation leads to cellular hypoxia

To determine whether high glucose metabolism leads to cellular hypoxia, we cultured isolated C57BL/6J mouse pancreatic islets in the presence of 22 mM glucose, treated with the GCK activator GKA50, or both (Fig. 2G; quantification in fig. S1A). All these experimental conditions led to an increase in the formation of pimonidazole adducts, indicating cellular hypoxia. The formation of pimonidazole adducts occurs under low oxygen tension and requires reduced nicotinamide adenine dinucleotide/reduced nicotinamide adenine dinucleotide phosphate (NADH/NADPH) (*26*). To preclude that the increase in pimonidazole adduct formation was due to the acute rise in NADH observed in response to an increase in glucose concentration (*28*), we compared islets cultured at 22 mM glucose for 2 hours versus 8 hours (when NADH concentration is no longer elevated), adding pimonidazole only during the last 2 hours of culture. Under these conditions, a higher pimonidazole adduct formation at 8 hours versus 2 hours was observed (Fig. 2H and fig. S1B), indicating that the increase in adduct formation results from cellular hypoxia. To ascertain whether additional players involved in insulin secretion contribute to cellular hypoxia in response to high glucose metabolism, we treated islets with the GCK activator GKA50 in the presence of the Ca^{2+} channel inhibitor nifedipine (*29*) or the K^+ channel activator diazoxide (*30*). Nifedipine treatment did not prevent the formation of high amounts of pimonidazole adducts, whereas the presence of diazoxide reduced adduct formation (Fig. 2I and fig. S1C). These results indicate that an increase in intracellular Ca^{2+} concentration ($[Ca^{2+}]_i$) is not required to achieve cellular hypoxia in response to high glucose metabolism. In contrast, activation of the K^+ channel prevented high cellular hypoxia, reflective of the reduced glycolysis rate after diazoxide-induced rise in adenosine triphosphate concentration and subsequent inhibition of phosphofructokinase-1 (*31*). We confirmed that nifedipine or diazoxide treatment conditions had the expected impact on β cell function by analyzing changes in $[Ca^{2+}]_i$ in the presence of high concentrations of glucose (fig. S2). As expected, both compounds had a substantial impact on glucose-stimulated $[Ca^{2+}]_i$, whereas only nifedipine affected KCl-induced $[Ca^{2+}]_i$.

Increasing GCK activity leads to HIF-1α protein stabilization and induction of target gene expression

We next sought to determine whether high glucose metabolism leads to HIF-1α stabilization and activation. We treated C57BL/6J mouse islets with GKA50 or exposed them to 12% O_2 for a period of 20 hours. Our results showed that increasing GCK activity led to HIF-1α stabilization and increased GLUT1 protein abundance. Conversely, under conditions of high glucose metabolism, addition of the HIF-1α inhibitor PX-478 decreased HIF-1α and GLUT1 protein amounts (Fig. 3A). Induction of *Slc2a1* gene expression, encoding for GLUT1, as well as other HIF-1 target genes including insulin-like growth factor–binding protein 3 (*Igfbp3*), hexokinase 2 (*Hk2*), phosphoglycerate kinase 1 (*Pgk1*), and *Pdk1*, was also observed in islets treated with GKA50 (Fig. 3, B to F). In contrast, mRNA expression of *Ldha* and B-cell lymphoma-2-interacting protein 3–encoding *Bnip3*, which is up-regulated in islets in response to hypoxia, was not induced by GKA50 treatment (Fig. 3, G and H). Under these experimental conditions, *Gck* mRNA abundance was reduced compared to untreated islets (Fig. 3I). In islets treated with GKA50, inhibition of HIF-1α activity by PX-478 decreased the expression of *Slc2a1*, *Igfbp3*, *Hk2*, *Pgk1*, and *Pdk1* (Fig. 3, B to F). These results demonstrate that high glucose metabolism leads to stabilization and activation of HIF-1α and up-regulation of expression of several HIF-1α target genes. To investigate whether high glucose metabolism increased HIF-2α–dependent transcriptional activity in response to GKA50 treatment, we analyzed the expression of two genes known to be specifically up-regulated by HIF-2α. Expression of *Ccnd1* and *Pai1* was not up-regulated by either increased GCK activity or exposure to hypoxia (fig. S3). These observations suggest that HIF-2α activity has no major role in the pancreatic islet's response to either cellular or environmental hypoxia. Furthermore, previous studies showed that, in contrast to HIF-1α (*23*), overexpression of HIF-2α in β cells has no impact on glucose homeostasis (*32*). To ensure the absence of any negative impact of PX-478 on cell viability, we performed propidium iodide staining, which confirmed that, regardless of GKA50 cotreatment, treatment with PX-478 did not lead to an increase in cell death (fig. S4).

Treatment of mouse islets with the HIF-1α inhibitor PX-478 restores high glucose metabolism–dependent up-regulation of basal insulin secretion

To investigate the impact of HIF-1α inhibitor PX-478 on mouse islet function, we assessed insulin release in C57BL/6J mouse islets treated for 20 hours with the GCK activator in the presence or absence of the inhibitor. GCK activation led to a dose response–dependent increase in basal insulin secretion without affecting insulin release at high glucose concentration (Fig. 3J). The presence of the HIF-1α inhibitor substantially decreased basal insulin secretion to near control values with the consequent increase of the stimulation index (Fig. 3K), whereas insulin content remained unchanged (Fig. 3L). These results indicate that treatment of mouse islets under metabolic overload with PX-478 ameliorates β cell function by restoring glucose-dependent insulin secretion.

Because $[Ca^{2+}]_i$ acts as the main triggering signal linking glucose sensing/metabolism to insulin release (*30*), we next investigated how high glucose metabolism affects Ca^{2+} handling in β cells. Islets were treated with GKA50 for 20 hours and fasted in perifusion buffer containing 3 mM glucose for 2 hours before $[Ca^{2+}]_i$ recording (Fig. 3, M to Q). Islets that had gone through high metabolic activity displayed $[Ca^{2+}]_i$ oscillations already at basal low glucose concentration, and treatment with the HIF-1α inhibitor PX-478 prevented these basal $[Ca^{2+}]_i$ oscillations (Fig. 3R and fig. S5). Activation of GCK also led to a faster response to glucose that was not changed by

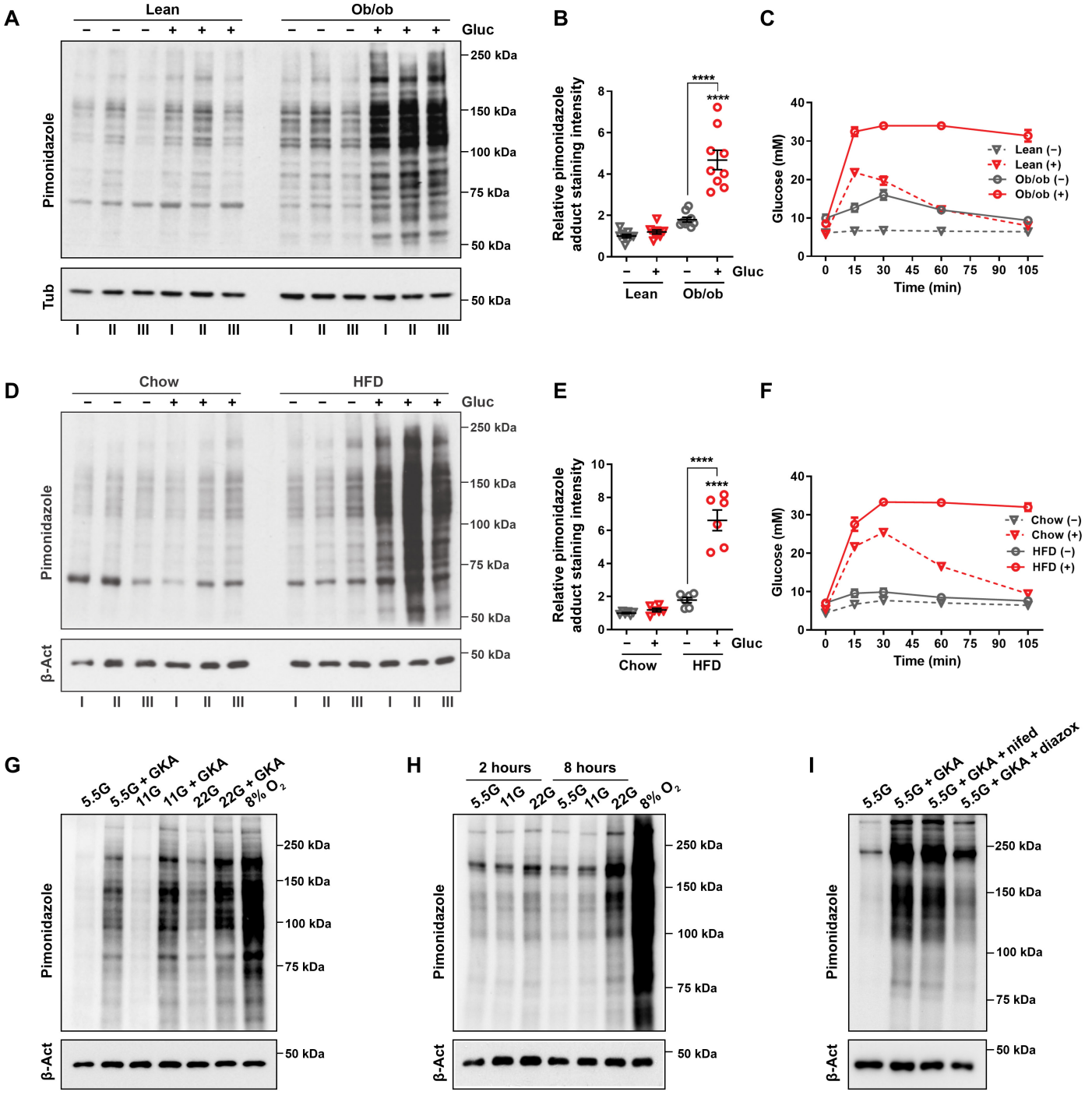

Fig. 2. Glucose loading leads to increased formation in vivo of pimonidazole adducts in islets of Langerhans from diabetic mouse models. Ob/ob mice (**A** to **C**) ($n = 9$ per group) and HFD-fed mice (**D** to **F**) ($n = 6$ per group) were injected with saline solution (–) or glucose (+). Results of three representative mice of each group are presented. Immunoblotting was performed using anti-pimonidazole adducts and anti-tubulin or anti–β-actin antibodies. (B and E) Quantification of pimonidazole adduct staining intensity. Results are presented as fold induction over the average of saline-injected lean (B) or chow-fed mice (E) run in the same SDS polyacrylamide gel. Two or three independent SDS polyacrylamide gels were run for each animal model of diabetes. (C and F) Blood glucose values after glucose loading. (**G** to **I**) In vitro studies with isolated C57BL/6J mouse islets showing the impact of glucose metabolism on pimonidazole adduct formation. (G) Islets cultured for 8 hours in the presence of 5.5 mM (5.5G), 11 mM (11G), or 22 mM (22G) glucose with or without GCK activator GKA50 (GKA) treatment. (H) Islets cultured for 2 or 8 hours at the indicated glucose concentrations. (I) Islets cultured for 8 hours in the presence of 5.5 mM glucose and GKA50 with or without cotreatment with nifedipine (nifed) or diazoxide (diazox). At the end of treatment, islets were lysed, and immunoblotting analysis was performed using anti-pimonidazole adduct and β-actin antibodies. Quantifications of staining intensities for (G) to (I) are provided in fig. S1. ****$P < 0.0001$ by two-way analysis of variance (ANOVA) with Tukey's multiple comparisons test.

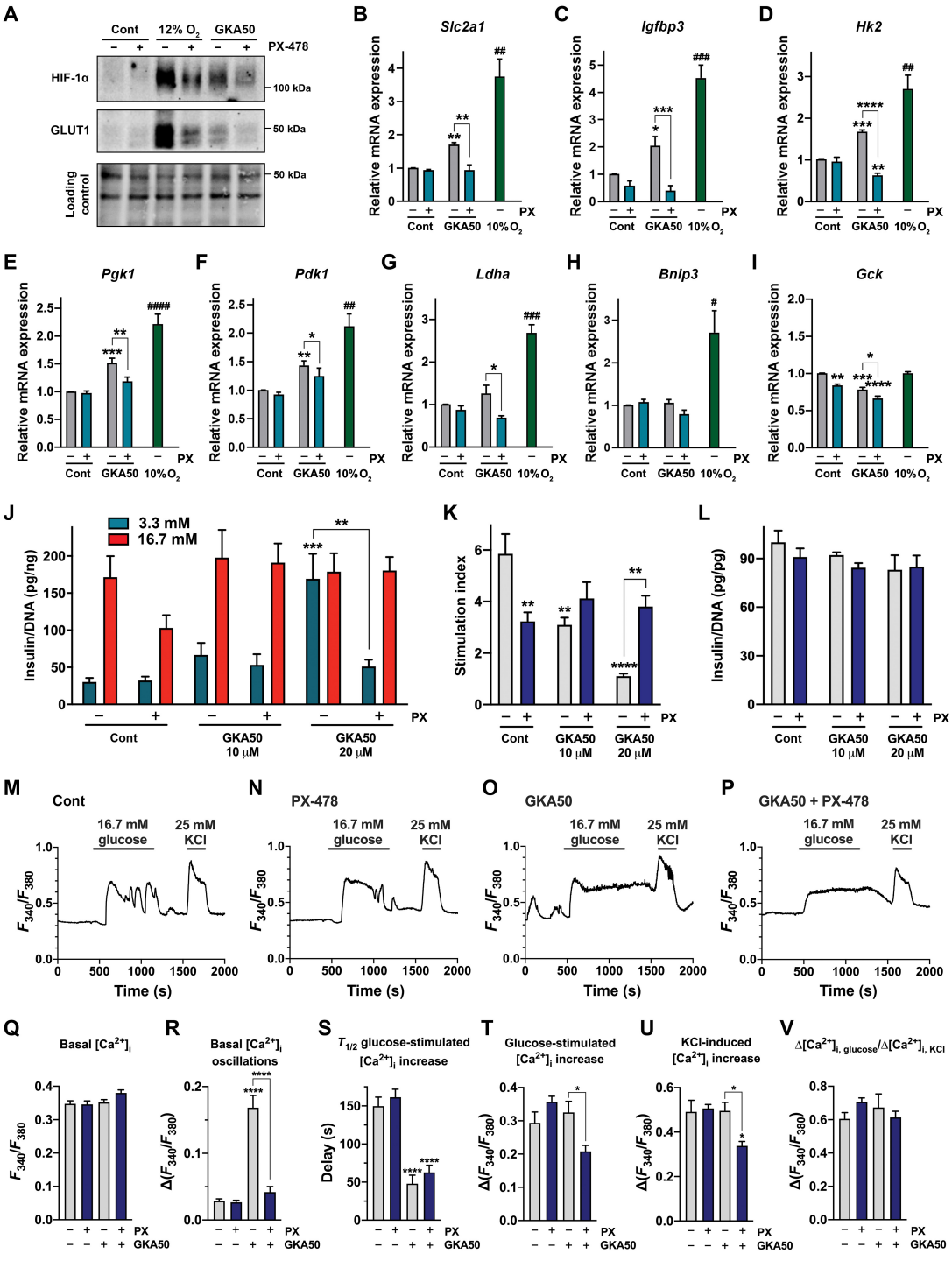

Fig. 3. Under high glucose metabolism, treatment with the HIF-1α inhibitor PX-478 restores basal insulin secretion and prevents the emergence of $[Ca^{2+}]_i$ oscillations at low glucose. Islets from C57BL/6J mice were either treated with GCK activator (GKA50; 20 μM unless otherwise specified), exposed to hypoxia, or left untreated (cont) in the presence or absence of PX-478. (**A**) Protein abundance of HIF-1α and GLUT1. Loading control was performed using the ChemiDoc stain-free imaging system. (**B** to **H**) Gene expression of HIF-1α target genes *Glut1* (B), *Igfbp3* (C), *Hk2* (D), *Pgk1* (E), *Pdk1* (F), *Ldha* (G), *Bnip3* (H), and expression of *Gck* (**I**) analyzed by qRT-PCR. Gene expression from three to four independent experiments was analyzed. For each experiment, islet preparations of three mice were pulled together. (**J**) Assessment of insulin release by static batch incubation of islets ($n = 5$). (**K**) Stimulation index. (**L**) Insulin content. (**M** to **P**) Representative traces of $[Ca^{2+}]_i$ of islets treated with PX-478 ($n = 6$) (N), GKA50 ($n = 8$) (O), GKA50 + PX-478 ($n = 8$) (P), or control islets (cont) ($n = 7$) (M). (**Q** to **V**) Analysis of $[Ca^{2+}]_i$ traces as indicated. Statistical significance associated with brackets indicates differences between islets treated with PX-478 and their corresponding controls. $^*P < 0.05$, $^{**}P < 0.01$, $^{***}P < 0.001$, and $^{****}P < 0.0001$ by two-way ANOVA with Tukey's multiple comparisons test. $\#P < 0.05$, $\#\#P < 0.01$, $\#\#\#P < 0.001$, and $\#\#\#\#P < 0.0001$ by two-tailed unpaired Student's *t* test to compare gene expression from islets exposed to hypoxia with untreated control islets.

PX-478 (Fig. 3S). Considering that islets were fasted 2 hours before changes in $[Ca^{2+}]_i$ were recorded, we conclude that the presence of basal $[Ca^{2+}]_i$ oscillations results from a change in islet phenotype. Although PX-478 treatment in the presence of the GCK activator decreased the rise of $[Ca^{2+}]_i$ in response to glucose (Fig. 3T), this did not have any deleterious effect on insulin secretion at high glucose concentration.

PX-478 prevents the rise of glycemia in db/db mice

The db/db mouse is an extreme model of obese type 2 diabetes, characterized by early loss of β cell function. Db/db mice present hyperinsulinemia at an early age followed by β cell failure that leads to persistent hyperglycemia at 2 to 3 months of age (*33*, *34*). In addition, freshly isolated islets from these animals have high basal insulin secretion and $[Ca^{2+}]_i$ oscillations at low glucose (*35*, *36*).

In this context, we investigated the impact of the HIF-1α inhibitor PX-478 on the progression of diabetes in this mouse model. At 6 weeks of age, db/db mice started receiving PX-478 (30 mg/kg) or phosphate-buffered saline (PBS) by intraperitoneal injection, twice per week (Fig. 4A). The body weight of treated and nontreated db/db mice both increased during the experimental period, without any statistically significant difference between the two groups of animals (Fig. 4B). In nontreated db/db mice, nonfasting blood glucose rose from 5 to 9 weeks of age and remained high afterwards (Fig. 4C). This increase in glycemia was not observed when we treated db/db mice with the HIF-1α inhibitor. In addition, 5-week-old db/db mice were hyperinsulinemic, with plasma insulin values 10- to 15-fold higher than db/+ control mice (Fig. 4D). In untreated db/db mice, plasma insulin concentration dropped in an age-dependent manner, whereas mice treated with PX-478 sustained elevated insulin concentrations until the end of the experiment. These results suggest that, in treated mice, pancreatic β cells maintain the ability to secrete high amounts of insulin that compensate for the high insulin resistance that characterizes this mouse model (*33*).

To further characterize the metabolic state of these animals, we performed glucose and insulin tolerance tests. Db/db mice treated with PX-478 showed better tolerance to glucose (Fig. 4, E and F), higher plasma insulin concentrations (Fig. 4G), and improved values of homeostatic model assessment (HOMA) for β cell function (HOMA-β) (Fig. 4H). No improvement in peripheral insulin sensitivity was observed in treated mice, as indicated by the area under the curve of the insulin tolerance test and the HOMA for insulin resistance (HOMA-IR) (Fig. 4, I and J). In glucose and insulin tolerance tests, treated animals presented fasting blood glucose values close to db/+ controls, whereas their plasma insulin was twofold higher than nontreated db/db mice. Considering that PX-478–treated mice did not show an improvement in insulin sensitivity, the data indicate that better tolerance to glucose is a consequence of the observed elevated plasma insulin concentration and improved β cell function.

To assess the impact of PX-478 treatment on peripheral tissues, we analyzed the expression of genes involved in pathways relevant for adipocyte function and insulin sensitivity in visceral and subcutaneous white adipose tissue (WAT) of db/db mice. Among the genes investigated, only *Ucp1* and *Fasn* expressions in visceral WAT were restored to values observed in lean mice after treatment with PX-478 (fig. S6). This result indicates that PX-478 treatment does not improve insulin-mediated regulation of the lipogenic pathway (*37*). No changes in gene expression were observed in subcutaneous WAT (fig. S7). Furthermore, in visceral WAT, *Acc1* expression was not restored and *Dgat1* mRNA abundance was down-regulated in treated versus nontreated mice. Expression of liver genes was also analyzed regarding glucose and lipid metabolism. No major impact on lipid metabolism was observed in the liver of db/db mice treated with PX-478. In contrast, up-regulation of *Gck* and inhibition of *Pdk4* and *G6Pase* expression indicated a potential positive impact of PX-478 on liver glucose metabolism (fig. S8).

To evaluate the impact of PX-478 treatment in an obesity-driven insulin resistance mouse model without collapse of β cell function, we treated HFD-fed mice over a period of 4 weeks with two different doses of the HIF-1α inhibitor (fig. S9A). Treatment with the lower dose of PX-478 (30 mg/kg body weight) prevented the increase in weight in response to HFD feeding, whereas substantial weight loss was observed in mice treated with a dose of 45 mg/kg body weight (fig. S9, B and C). Nonfasting blood glucose did not differ between groups of mice (fig. S9D). In contrast, nonfasting plasma insulin concentrations were increased in HFD-fed mice as compared to lean mice, whereas treatment of HFD-fed mice with PX-478 led to a decrease in insulin values (fig. S9E). Tolerance to glucose was slightly ameliorated in HFD-fed treated mice compared to nontreated mice (fig. S9, F and G), and this improvement was accompanied by lower values of fasting plasma insulin (fig. S9H). Treatment with PX-478 (45 mg/kg) improved insulin tolerance and decreased HOMA-IR (fig. S9, I to K). These results led us to conclude that, in HFD-fed mice, the HIF-1α inhibitor improves insulin sensitivity. Whereas improvement in glucose tolerance mediated by PX-478 in HFD-fed mice was accompanied by lower fasting insulin values that correlated with better insulin sensitivity, in db/db mice, treatment produced higher fasting insulin values and no improvement of insulin resistance.

Treatment of db/db mice with PX-478 improves β cell proliferative capacity

It has been previously shown that the increase in glycemia in these mice is accompanied by a severe reduction in the rate of β cell proliferation (*33*). To further investigate the impact of PX-478 on the endocrine pancreas, we analyzed the proliferation rate of β cells in db/db mice. Compared to untreated mice, animals treated with the HIF-1α inhibitor presented a higher rate of β cell proliferation, as assessed by Ki67 staining (Fig. 5, A and B). These results suggest that PX-478 treatment prevented the decrease in β cell proliferation rate usually observed in db/db mice. We also investigated the ratio of α, β, or δ cells in PX-478–treated or nontreated db/db mice. The area of each distinct endocrine cell type was different in islets present in the gastric/duodenal part of the pancreas compared to the splenic region (Fig. 5, C to I). Islets of animals treated with PX-478 showed, in both parts of the pancreas, increased β cell area with a concomitant reduction in α and δ cell areas. These observations suggest that, by preserving β cell function, PX-478 might increase the ability to expand β cell mass in db/db mice.

PX-478 decreases glycemia and HbA1c in STZ-induced diabetic mice

Given the potential beneficial effect of PX-478 on β cell function, we next investigated whether PX-478 could improve glycemia in an insulin resistance–independent model of diabetes wherein hyperglycemia is driven by a reduction in functional β cell mass (*38*, *39*). To this aim, we used the STZ-induced diabetic mouse model. A low dose of toxin was administered daily for five consecutive days to C57BL/6J mice (Fig. 6A). Thirteen days after the last administration of the toxin, STZ-induced diabetic mice started receiving either PX-478 (40 mg/kg) or PBS. During the experimental period, body weights of treated and nontreated mice were similar (Fig. 6B). At the beginning of treatment, both groups of STZ mice presented blood glucose concentrations between 15 and 25 mM (Fig. 6C and fig. S10). In mice treated with PX-478, glycemia started to improve during the first week of treatment and remained lower than in nontreated mice. At the end of the study, PX-478–treated mice predominantly presented blood glucose concentrations of less than 15 mM (Fig. 6C and fig. S10). In contrast, hyperglycemia persisted in nontreated mice, with most of the animals showing concentrations of blood glucose above 20 mM during the last week of the experimental period. After 6 weeks of treatment, hemoglobin A1c (HbA1c) values were assessed in all groups. HbA1c values for PX-478–treated STZ mice were comparable to values for control mice and lower than in

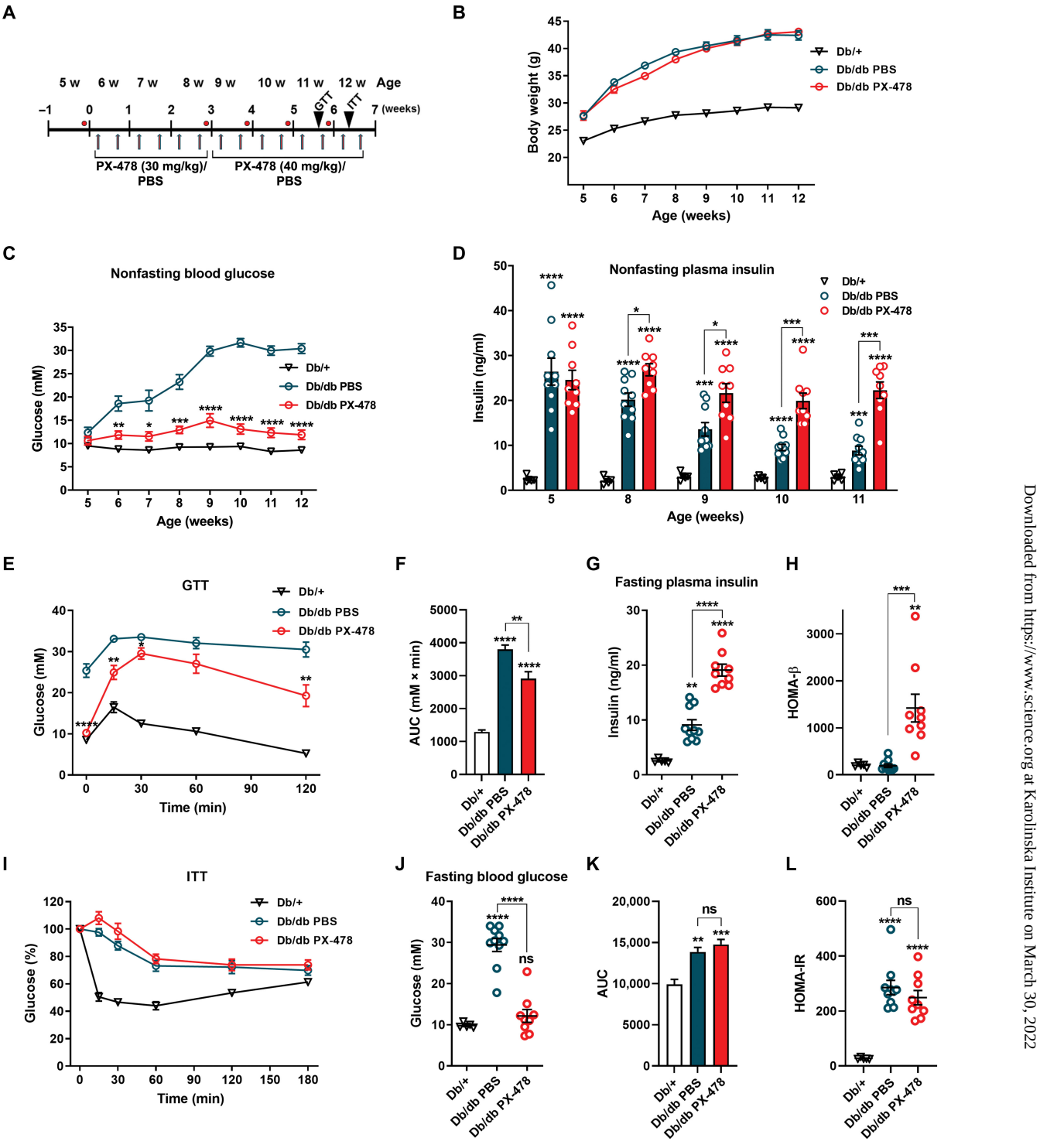

Fig. 4. Treatment of db/db mice with the HIF-1α inhibitor PX-478 prevents progression of diabetes. (**A**) Schematic representation of the intervention strategy indicating the number of weeks of treatment, age of the animals, and doses of PX-478 administered. Db/db mice were treated with PX-478 ($n = 9$) or injected with PBS ($n = 10$) twice a week as indicated. Normoglycemic control db/+ ($n = 5$) were also injected with PBS. Red dots indicate the days when blood was collected to measure nonfasting plasma insulin concentration. Glucose tolerance test (GTT) or insulin tolerance test (ITT) was performed at indicated weeks (arrowheads). (**B**) Body weight. (**C**) Nonfasting blood glucose. (**D**) Nonfasting plasma insulin. (**E**) GTT. (**F**) Area under the curve of GTT. (**G**) Fasting plasma insulin. (**H**) HOMA-β. (**I**) ITT. (**J**) Fasting blood glucose of ITT. (**K**) Area under the curve of ITT. (**L**) HOMA-IR. (E to J) Mice were fasted for 6 hours. *$P < 0.05$, **$P < 0.01$, ***$P < 0.001$, and ****$P < 0.0001$ by one-way ANOVA with Tukey's multiple comparisons test (F to H and J to L) and by two-way ANOVA with Tukey's multiple comparisons test (B to E and I). Statistical significances displayed in (C), (E), and (I) indicate differences between db/db treated and nontreated groups. ns, not significant.

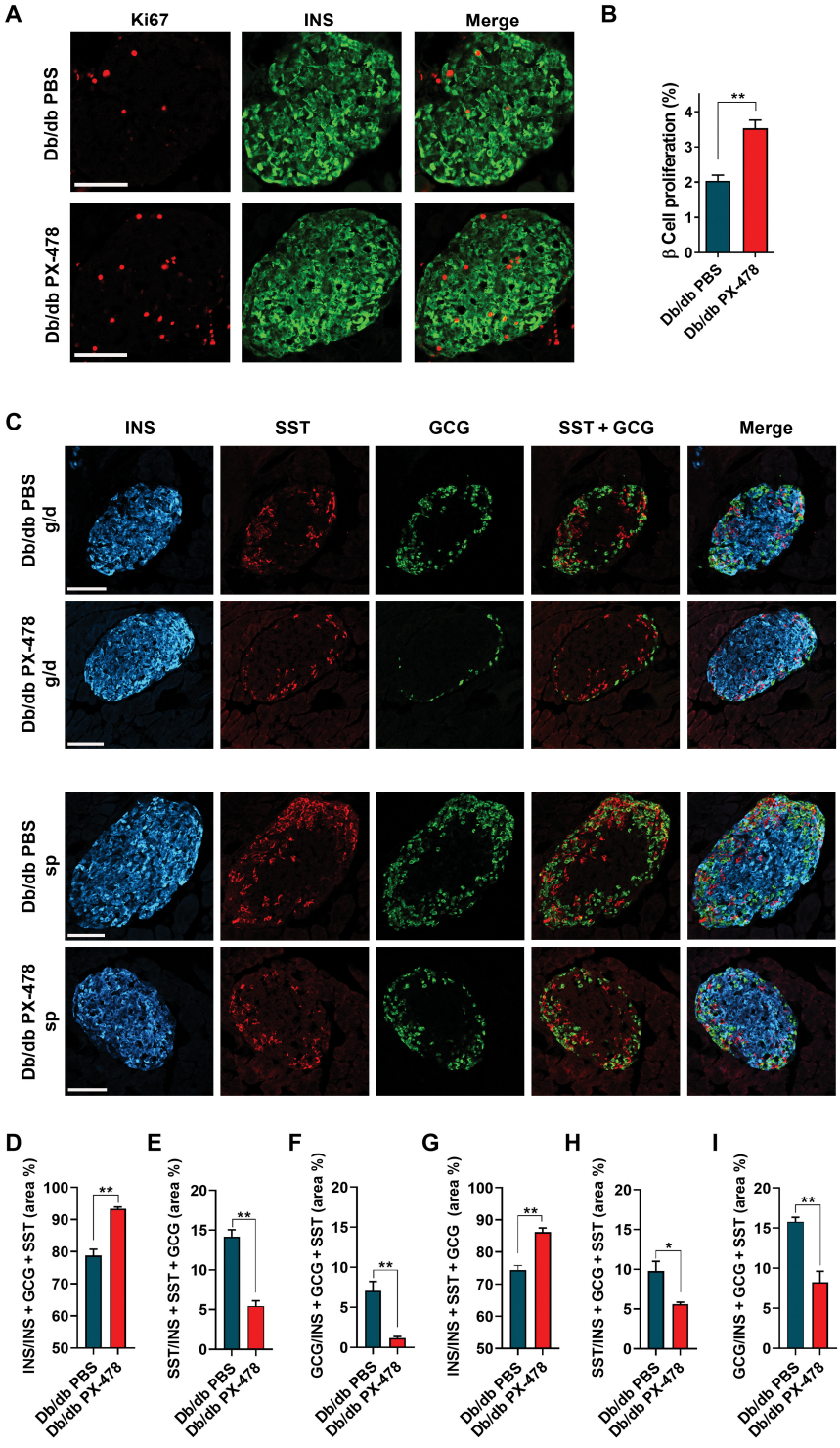

Fig. 5. Treatment of db/db mice with PX-478 leads to an increase in β cell proliferation rate and β cell area. (**A**) Detection of Ki67-positive cells by immunocytochemistry in pancreatic islets of db/db mice treated with the HIF-1α inhibitor (db/db PX-478) and in nontreated db/db mice (db/db PBS). Frozen sections were incubated with anti-Ki67 and anti-insulin (INS) antibodies. Imaging was performed using confocal microscopy. (**B**) Quantification of Ki67-positive cells in islets of db/db mice. Pancreata of PX-478–treated ($n = 4$) and nontreated ($n = 4$) db/db mice were used in this study. Eleven to 16 islets were imaged per mouse. (**C**) Immunocytochemistry of insulin (INS)–, somatostatin (SST)–, and glucagon (GCG)–positive cells in the gastric/duodenal (g/d) or splenic (sp) region of db/db mice pancreata. (**D** to **I**) Quantification of the area of INS-, SST-, and GCG-positive cells in the gastric/duodenal (D to F) or splenic (G to I) region of db/db pancreata. Pancreata of PX-478–treated ($n = 3$) and nontreated ($n = 3$) db/db mice were used in this study. Ten islets of each region, gastric/duodenal or splenic of the pancreas, were imaged per mouse. Scale bars, 100 μm. $^*P < 0.05$ and $^{**}P < 0.01$ by two-tailed unpaired Student's *t* test.

nontreated STZ animals (Fig. 6D). These results are in agreement with improved HOMA-β assessed after the same period of treatment (Fig. 6E).

Metabolic characterization of the STZ-induced diabetic mice showed that PX-478 improved tolerance to glucose, with treated mice presenting lower fasting blood glucose compared to nontreated animals (Fig. 6, F and G). Fasting plasma insulin concentrations in the PX-478–treated group were twofold higher than in nontreated mice, and insulin values remained higher during all the time points of the glucose tolerance test, leading to a statistically significant increase of the area under the curve ($P < 0.0001$) (Fig. 6, H and I). These observations suggest that increased glucose sensitivity is a consequence of higher concentration of plasma insulin. In agreement with this, no differences in insulin sensitivity and HOMA-IR were observed in treated and nontreated mice (Fig. 6, J to M).

PX-478 improves β cell function in STZ-induced diabetic mice

To better understand the impact of PX-478 on β cell function, animals were sacrificed 2 to 4 days after the last treatment, and pancreatic islets were isolated and analyzed. As expected, insulin content was substantially reduced in nontreated STZ mice compared to control animals (Fig. 7A) (*39*). PX-478 treatment had a positive impact on insulin content, resulting in a twofold increase. Analysis of gene expression in STZ mice showed a reduction in the expression of insulin genes *Ins1* and *Ins2* as compared to control mice (Fig. 7B). In contrast, the expression of genes encoding other endocrine hormones was up-regulated in STZ mice. Treatment with PX-478, although having no additional impact on insulin gene expression, decreased the expression of the other hormone-encoding genes analyzed. Comparing PX-478–treated to nontreated mice, down-regulation of glucagon (*Gcg*) and somatostatin (*Sst*) expression did not reflect a reduction in α or δ cell areas (fig. S11, A to C). Both PX-478–treated and nontreated STZ-induced diabetic mice presented an increase in α and δ cell areas as compared to control animals, and the changes in islet

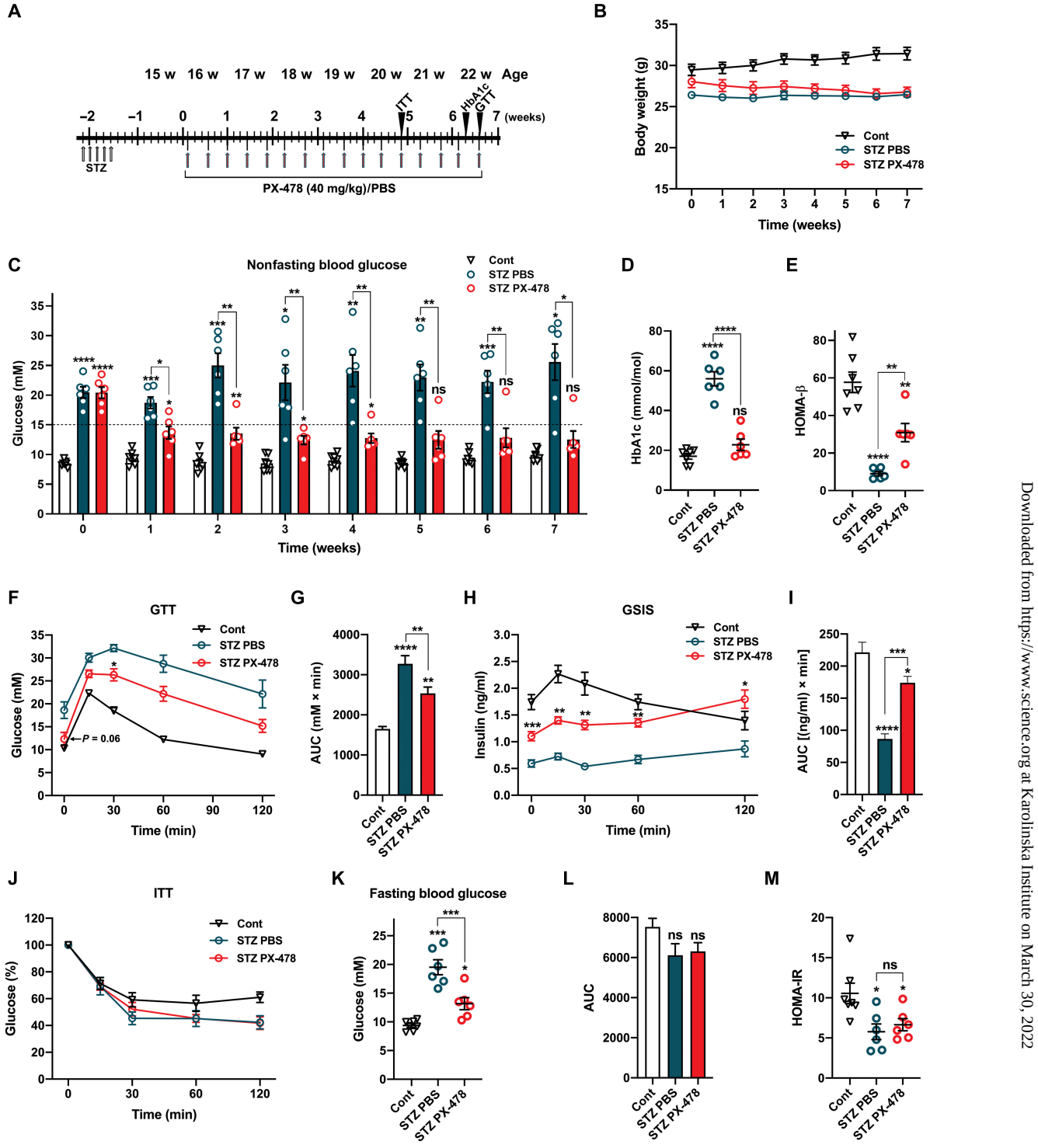

Fig. 6. Improvement of glycemia and HbA1c is observed in STZ-induced diabetic mice treated with PX-478. (**A**) Schematic representation of the intervention strategy indicating number of weeks of treatment, age of the animals, and dose of PX-478 administered. STZ mice were treated with PX-478 ($n = 6$) or injected with PBS ($n = 6$) as indicated. Control mice ($n = 6$) were also injected with PBS. GTT, ITT, or HbA1c assessments were performed at the indicated days (arrowheads). (**B**) Body weight. (**C**) Nonfasting blood glucose. (**D**) HbA1c. (**E**) HOMA-β. (**F**) GTT. (**G**) Area under the curve of GTT. (**H**) Glucose-stimulated insulin secretion (GSIS). (**I**) Area under the curve of GSIS. (**J**) ITT. (**K**) Fasting glucose of ITT. (**L**) Area under the curve of ITT. (**M**) HOMA-IR. Statistical analyses were performed between treated and nontreated STZ-induced diabetic groups for (B), (F), (H), and (J). (F to M) Mice were fasted for 6 hours. *$P < 0.5$, **$P < 0.01$, ***$P < 0.001$, and ****$P < 0.0001$ by one-way ANOVA with Tukey's multiple comparisons test (D, E, G, I, and K to M) and by two-way ANOVA with Tukey's multiple comparisons test (B, C, F, H, and J). Statistical significances displayed in (F), (H), and (J) indicate differences between STZ-induced treated and nontreated groups.

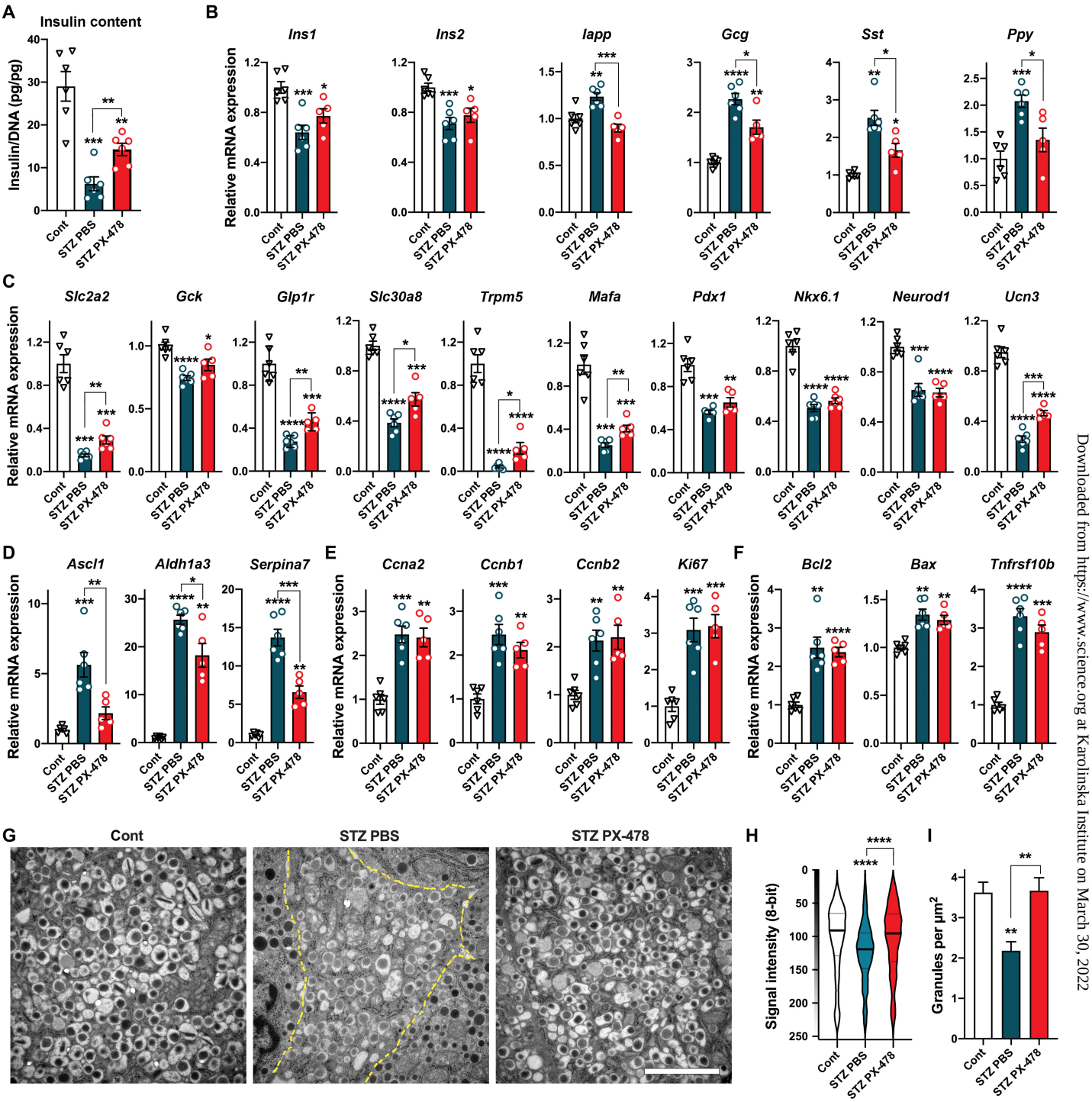

Fig. 7. Insulin content values, gene expression analysis, and maturity of insulin granules indicate improvement of β cell function in STZ-induced diabetic mice after PX-478 treatment. (**A**) Islet insulin content from PX-478–treated ($n = 6$) or nontreated ($n = 6$) STZ-induced diabetic mice and their normoglycemic controls ($n = 6$). (**B** to **F**) Analysis of gene expression by qRT-PCR of freshly isolated islets from PX-478–treated ($n = 5$) or nontreated ($n = 6$) STZ mice and their nondiabetic controls ($n = 6$). Expression of genes encoding pancreatic islet hormones (B), genes involved in β cell function and maturity (C), markers of β cell metabolic stress and dedifferentiation (D), markers of proliferation (E), and genes involved in apoptosis (F) is presented. (**G**) Representative electron microscopy images of pancreatic β cells from control ($n = 6$), STZ PBS ($n = 4$), and STZ PX-478 ($n = 5$), as well as quantifications for granule opacity (**H**) and density (**I**). Dashed yellow line in (G) delineates a β cell. Scale bar, 2 µm. *$P < 0.5$, **$P < 0.01$, ***$P < 0.001$, and ****$P < 0.0001$ by Brown-Forsythe and Welch ANOVA tests.

architecture typically observed in STZ mice were not altered by PX-478 treatment.

We next investigated the expression of genes involved in β cell function and maturity that are down-regulated in STZ mice (*39*). PX-478 treatment resulted in increased expression of several of the analyzed genes including *Slc2a2*, *Glp1r*, *Slc30a8*, *Trpm5*, *Mafa*, and *Ucn3* (Fig. 7C). The expression of dedifferentiation markers that were augmented in STZ mice (*39*) was additionally analyzed. Expression of *Ascl1*, *Aldh1a3*, and *Serpina 7* were down-regulated by PX-478 treatment (Fig. 7D). These results suggest that PX-478 may have a positive impact on β cell function by up-regulating the expression of genes involved in function and maturity and by inhibiting dedifferentiation markers. In contrast, genes driving proliferation and apoptosis that are increased in STZ mice (*39*) were not affected by PX-478 treatment (Fig. 7, E and F). Last, transmission electron microscopy imaging was performed to assess the ultrastructural changes in STZ mice (Fig. 7, G to I). As previously shown, STZ-induced diabetic mice presented immature insulin granules instead of the typically dense granules containing crystallized insulin observed in control mice (*39*, *40*). Treatment of STZ mice with PX-478 promoted the formation of dark insulin granules similar to those of control mice (Fig. 7, G and H) and led to an increase in the number of granules per area unit (Fig. 7I). In conclusion, our analysis of freshly isolated islets demonstrated the positive impact of PX-478 on insulin content, gene expression, and formation of mature insulin granules, all together promoting an increased β cell function.

PX-478 increases the stimulation index of glucose-induced insulin secretion in human islet organoids chronically exposed to high glucose

To assess whether PX-478 improves the function of human β cells under high metabolic workload, we performed experiments using human islet organoids. Similarly to what has been observed with human islets, prolonged exposure of human islet organoids to high glucose concentrations leads to a marked up-regulation of basal insulin secretion with the correspondent collapse of the stimulation index (*41*, *42*). However, when cultured at normal glucose concentrations, human islet organoids have the advantage, when compared to native human islets, to display higher responses to glucose in terms of insulin secretion (*43*). To investigate the impact of PX-478 on human β cell function, we performed batch insulin assays after 15 days of culturing islet organoids in the presence of either 5.5 or 16.7 mM glucose. We used human islet organoids prepared from islets of three distinct donors (MT-171, MT-172, and MT-173) of the same gender and with similar body mass index (BMI) values (tables S2 and S3). Islet organoids cultured at 5.5 mM glucose presented low basal insulin secretion with a release at low glucose of 20 to 22 pg of insulin per islet. At high glucose, insulin secretion was strongly stimulated, reaching values of 165 to 570 pg of insulin per islet (Fig. 8, A and B). Treatment with PX-478 had no impact on insulin release of islet organoids cultured at 5.5 mM glucose. Human islet organoids cultured for 2 weeks in the presence of 16.7 mM glucose (Fig. 8, C and D) showed a robust increase of basal insulin secretion that was 7- to 9.5-fold higher compared to islet organoids cultured at 5.5 mM glucose. Increased basal insulin and reduced induction of insulin release in response to high glucose led to lower stimulation index values for islets cultured at 16.7 mM glucose (0.9- to 1.9-fold) compared to islets cultured at 5.5 mM glucose (9- to 26-fold) (Fig. 8, E and F). Treatment of islet organoids cultured at 16.7 mM glucose with PX-478 reduced basal insulin release and elevated stimulation indexes to 7.5-, 6.5-, and 4.8-fold in MT-171, MT-172, and MT-173, respectively (Fig. 8, E and F). In accordance with previous studies (*42*), insulin content was reduced by exposing islet organoids to high glucose (fig. S12, A and B). PX-478 treatment had no statistically significant impact on insulin content under conditions of high glucose metabolism (fig. S12, A and B) nor on human islet organoid cell number, as measured by DNA content cultured in either 5.5 or 16.7 mM glucose (fig. S12, A to D). The results of these studies show that PX-478 positively affects the function of human β cells under high metabolic overload by diminishing basal insulin secretion and increasing responsiveness to high glucose.

DISCUSSION

During the development of type 2 diabetes, pancreatic islets display a progressive increase in metabolic rate that acts as a compensatory mechanism to counteract insulin resistance. This sustained excessive metabolic pressure ultimately leads to β cell failure and to the inability to maintain normal blood glucose values. In the present study, we found that metabolic overload of mouse pancreatic islets led to the acquisition of a hypoxic phenotype and the dysregulation of insulin secretion. We show that, under metabolic overload, the HIF-1α inhibitor PX-478 restored normal insulin secretion in response to glucose in mouse islets and increased the stimulation index of glucose-induced insulin secretion in human islet organoids. We also demonstrate that treatment of db/db and STZ-induced diabetic mice with PX-478 decreased blood glucose concentration and improved β cell function.

Previous studies have proposed that culturing islets in the presence of high glucose concentration promotes a state of cellular hypoxia (*15*, *16*). We observed higher amounts of pimonidazole adduct formation when culturing islets at 22 mM glucose. Moreover, our current results show that, in diabetic ob/ob mice, an acute rise in blood glucose concentration by glucose loading led to an increase in the formation of pimonidazole adducts, which indicates that the islets of these animals are sensing low O_2 concentrations, corroborating previous findings (*15*). Establishment of cellular hypoxia in response to glucose loading was also observed in the prediabetic HFD-fed mouse model. These results indicate that, rather than being correlated with the stage of the disease, appearance of cellular hypoxia is associated with the level of intolerance to glucose.

Several publications have shown that, when islets or insulin-producing cells are exposed to concentrations of 1 to 5% oxygen, hypoxia mediates β cell death (*27*, *44*). These values of oxygen are relevant to situations of ischemic disease or islet transplantation. In contrast to these drastic low values of oxygen that can induce cell death, the degree of glucose metabolism–induced cellular hypoxia in our experimental settings corresponds to a much milder pathological hypoxia (above 10 to 12% oxygen).

HIF-1α degradation is strictly dependent on the interaction with VHL, which can only happen at normal O_2 concentrations (*18*–*20*). Studies in which the *Vhl* gene was deleted in β cells, either during embryonic development or in adult mice, have illustrated that sustained overexpression of HIF-1α leads to β cell dysfunction and results in a diabetogenic phenotype (*23*, *45*, *46*). In contrast with VHL knockout lineages, contradictory conclusions were reached in studies investigating the impact of ablating either HIF-1α or the HIF-1α dimerization partner Arnt on β cell function (*23*, *47*–*49*).

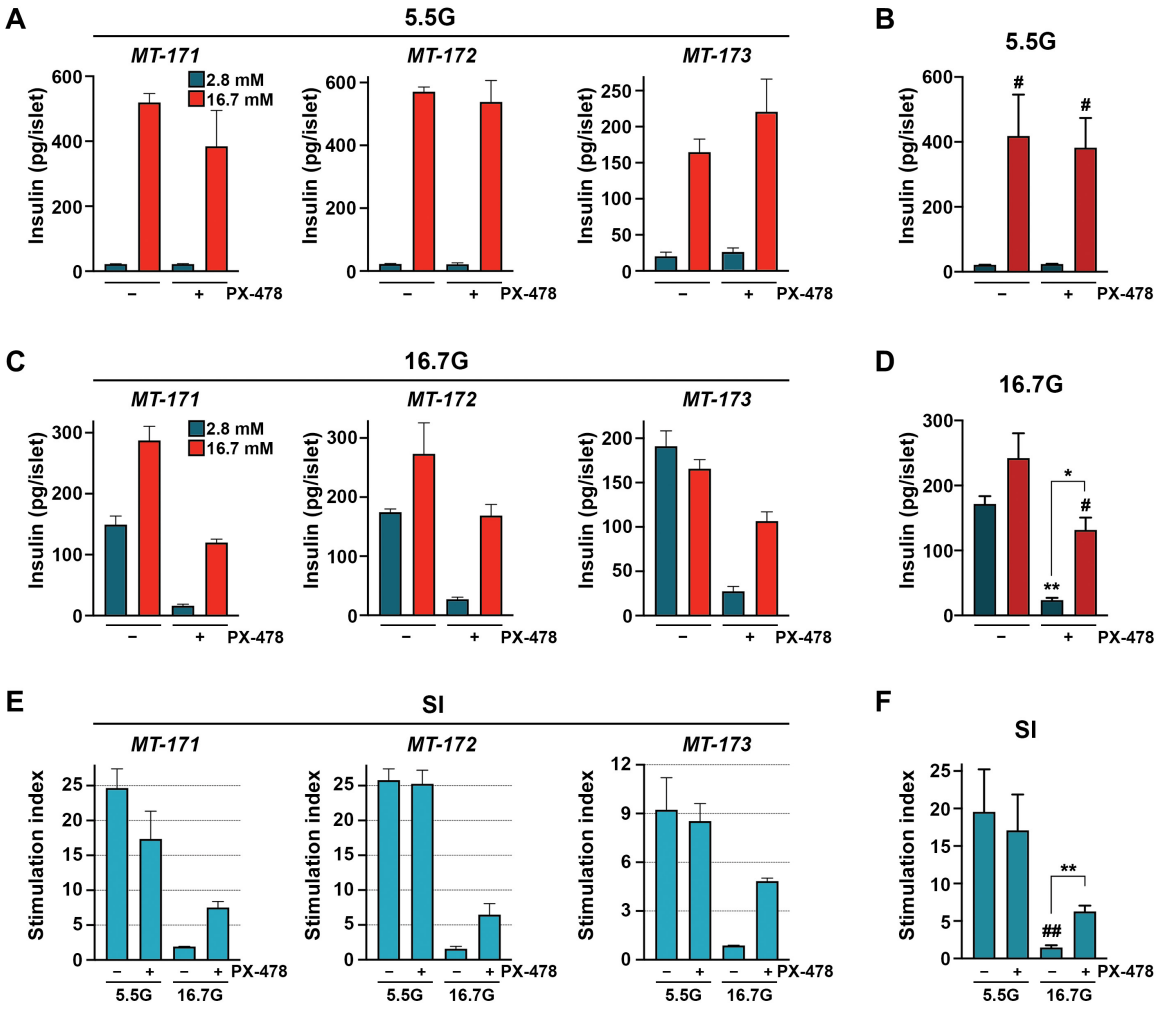

Fig. 8. PX-478 positively affects human islet organoids chronically exposed to high glucose by reducing basal insulin secretion and increasing stimulation index. Insulin release assays of islet organoids prepared from islets of individual donors (*MT-171*, *MT-172*, and *MT-173*) were conducted. Human islet organoids were cultured for 15 days in the presence of 5.5 mM (5.5G) (**A** and **B**) or 16.7 mM (16.7G) (**C** and **D**) glucose and treated (+) or untreated (–) with 25 μM PX-478. Insulin release was assessed at low (2.8 mM) and high (16.7 mM) glucose. (**E** and **F**) Stimulation index (SI). Bar plots at the end of each row show the average of the three individual experiments presented in that row. Statistical significance indicated by asterisks not associated with brackets represents analyses performed between islet organoids and (B and D) untreated islet organoids at 2.8 mM glucose or (F) untreated 5.5G islet organoids. $*P < 0.05$ and $**P < 0.01$ by repeated measures one-way ANOVA with Fisher's multiple comparisons test; $\#P < 0.05$ and $\#\#P < 0.01$ by two-tailed paired Student's *t* test to compare values at 16.7 mM versus 5.5 mM glucose, with or without PX-478.

Considering the results of the present study and the current consensus regarding the diabetic phenotype of multiple VHL knockout mouse lines (*23*, *45*, *46*), we propose that up-regulation of HIF-1α protein abundance is deleterious to β cell function and can contribute to diabetes.

In the present study, we have inquired whether an increase in glucose metabolism could also lead to cellular hypoxia in a glucose concentration–independent manner. Our in vitro results show that increasing the glycolytic flux by activation of GCK drives pancreatic islets to a state of cellular hypoxia that is sufficient to stabilize HIF-1α and enhance the expression of several of its target genes. Under these experimental conditions, treatment with the HIF-1α inhibitor PX-478 down-regulated the expression of several HIF-1α target genes. We have also assessed the impact of the HIF-1α inhibitor PX-478 on insulin secretion at conditions of high glucose metabolism. Here, we observed an increase in basal insulin release, which was abrogated by the HIF-1α inhibitor PX-478. Our studies show that high glucose metabolism up-regulates several HIF-1α target genes including the genes encoding the high-affinity glucose transporter GLUT1 and the glycolytic enzymes PGK1, PDK1, and HK2. When compared to GCK, HK has a much higher binding affinity to glucose and is not regulated through negative feedback inhibition by glucose-6-phosphate. Therefore, an increased expression of HK can lead to a rise in glycolytic flux (*50*), leading to an increase in insulin secretion at low glucose (*51*). Under the experimental conditions used in our study, high glucose metabolism up-regulates *Hk2* and inhibits *Gck* expression. The change in the ratio of these enzymes together with an increase in GLUT1 abundance may increase glycolytic flux and drive high basal insulin secretion. GLUT1 displays a much higher affinity to glucose than GLUT2 (*52*); thus, increasing amounts of GLUT1 will lead to a lower threshold of glucose concentration for cellular uptake and, thereby, to an increase in glucose metabolism. Accordingly,

we found that inhibition of HIF-1α activity with PX-478 reduces *Glut1* and *Hk2* expression. Although we cannot exclude the participation of other pathways, our studies suggest that HIF-1α–dependent activation of transcription is necessary to achieve high basal insulin secretion under high glucose metabolism.

The early compensatory stage of obesity-linked type 2 diabetes is characterized by β cell hypertrophy and hyperplasia, and by a leftward shift in the glucose dose-response curve of insulin secretion (*53*). This lower set point of insulin secretion is associated with the occurrence of $[Ca^{2+}]_i$ oscillations (*35*). $[Ca^{2+}]_i$ oscillations at low glucose concentrations are also observed in freshly isolated islets of db/db mice or islets of lean mice cultured overnight in the presence of high glucose (*35*, *53*). In our study, we show that $[Ca^{2+}]_i$ oscillations result from high glucose metabolism. We postulate that the HIF-1α target genes up-regulated in pancreatic islets in response to high glucose metabolism increase the glycolytic flux at low glucose, driving the appearance of $[Ca^{2+}]_i$ oscillations and leading to high basal insulin secretion. Treatment with the HIF-1α inhibitor PX-478 prevents the emergence of $[Ca^{2+}]_i$ oscillations at low glucose and consequently restores basal insulin secretion.

Because we demonstrated that, under metabolic overload, the HIF-1α inhibitor PX-478 improves β cell function, we investigated the impact of PX-478 treatment in two diabetic mouse models, db/db and STZ-induced diabetic mice. The db/db mouse is an obesity-linked diabetic model presenting severe insulin resistance that leads to high metabolic overload and subsequent β cell exhaustion and failure (*33*, *34*). The STZ-induced diabetic mouse is a lean model of reduced functional β cell mass in which β cells are under high metabolic workload (*39*). In both models, treatment with PX-478 led to ameliorated blood glucose values compared to untreated mice. In db/db mice, PX-478 treatment averted the rise in blood glucose concentration by sustaining elevated insulin values and therefore preventing diabetes progression. In STZ mice, PX-478 reduced hyperglycemia and decreased HbA1c values. In both diabetic mouse models, improvement of glucose tolerance was associated with higher concentration of fasting plasma insulin, elevated HOMA-β, and no changes in insulin sensitivity. These observations suggest that PX-478–mediated improvement of glycemia results from ameliorated β cell function.

We have recently shown that β cell dysfunction is a major contributor to the phenotype of STZ-induced diabetic mice (*39*). Transplantation of islets into the anterior chamber of the eye of these animals, leading to a reduction of hyperglycemia and thereby to a decreased metabolic overload, mediated improvement of β cell function without affecting β cell mass. Islets located in the pancreata of transplanted mice displayed the same hallmarks of increased β cell function that were observed in the current study with STZ mice treated with PX-478, indicating that PX-478 has a positive impact on β cell function and maturity. In contrast to pancreatic islets from STZ mice rendered normoglycemic by islet transplantation, expression of proliferation and apoptosis markers was not down-regulated in PX-478–treated animals, suggesting that these islets are metabolically more active than those in the pancreas of transplanted mice (*39*). We have also observed that the gene expression of endocrine hormones that are up-regulated in STZ mice (*54*) was partially restored by PX-478 treatment. Although the mechanism mediating down-regulation of *Gcg*, *Sst*, and *Ppy* in PX-478–treated STZ mice remains to be investigated, we speculate that this inhibition might contribute to an improvement of islet phenotype.

Glucose-lowering therapeutic strategies such as sodium/glucose cotransporter (SGLT-2) inhibitors have been shown to protect β cell function in db/db mice. SGLT-2 inhibitors reduce β cell overload by increasing urinary excretion of glucose. SGLT-2 inhibitor–treated db/db mice present many similarities with the PX-478–mediated phenotype, including improvement of glycemia with the maintenance of high levels of nonfasting insulin, higher β cell proliferation rate, increased β cell area ratio, and decreased α cell area ratio (*55*–*58*). Furthermore, no changes in body weight were observed in either intervention. These observations suggest that, in analogy with the SGLT-2 inhibitor–mediated phenotype, the HIF-1α inhibitor PX-478 preserves β cell function in db/db mice.

Several studies have shown that, in obesity, the adipose tissue becomes hypoxic, and HIF-1α is a major contributor to inflammation and insulin resistance (*59*). In the prediabetic HFD-fed mouse model, disruption of HIF-1α or treatment with HIF-1α inhibitors such as with PX-478 or acriflavine has been shown to improve peripheral insulin sensitivity and promote weight loss (*59*–*61*). In our study, we confirmed that treatment of HFD-fed mice with PX-478 leads to better insulin sensitivity associated with lower fasting insulin concentration and weight loss in a dose-dependent manner. In contrast to HFD-fed mice, in db/db mice treated with PX-478, no major improvement in peripheral insulin sensitivity was observed. Because we selected a dose of PX-478 that does not affect body weight, we cannot exclude that higher doses of the HIF-1α inhibitor would affect insulin sensitivity and adiposity in db/db mice. However, in the current study, no major impact on adipose tissue gene expression was observed, ruling out a considerable contribution of this tissue to the observed phenotype. Analysis of the different mouse models indicates that in diabetic mice such as db/db and STZ animals, presenting high values of nonfasting glucose, PX-478 improves β cell function and glycemia. In prediabetic normoglycemic obese HFD-fed animals, where β cell function compensates for insulin resistance, the main impact of PX-478 treatment was on body weight and insulin sensitivity.

In contrast with the adipose tissue, the liver of db/db mice treated with PX-478 showed ameliorated glucose metabolism, with up-regulation of *Gck* and restoration of the expression of genes encoding gluconeogenic enzymes. Although inhibition of gluconeogenesis may contribute to better glycemia, the observation that db/db mice treated with HIF-1α inhibitor remain insulin resistant and hyperinsulinemic suggests that the compensatory β cell response promoting the release of high amounts of insulin is the main characteristic of the phenotype of PX-478–treated db/db mice.

We also investigated the ability of PX-478 to improve human β cell function in human islet organoids chronically exposed to high glucose. Prolonged exposure of human islets or islet organoids to high glucose leads to a marked increase of basal insulin secretion (*41*, *42*). Elevated fasting insulin is observed in obese, prediabetic, and some diabetic subjects (*6*, *7*, *62*, *63*). However, in islets isolated from these patients and cultured at a normal concentration of glucose, assessments of insulin release in vitro do not reconstitute the high fasting insulin values observed in vivo (*64*, *65*), suggesting that sustained high metabolic workload is necessary to mediate this dysfunctional β cell feature. In agreement with this hypothesis, a recent publication using pancreatic slides freshly prepared from prediabetic individuals has shown elevated insulin secretion at low glucose (*63*) that correlated with high fasting insulin concentrations in these patients. In analogy to the results obtained with mouse islets, PX-478

treatment of human islet organoids decreased basal insulin secretion with the concomitant positive impact on the stimulation index. These results suggest that PX-478 is able to preserve human β cell function under conditions of high metabolic workload. We speculate that lowering basal insulin values will help in preventing long-term β cell failure.

The main limitation of our studies is that translation of PX-478 effect from diabetic animal models to human islets was only assessed using in vitro experimental approaches. The impact of PX-478 on human pancreatic β cell function in vivo needs to be further investigated to fully assess the relevance of our studies to human health. Future experimental work studying the effect of PX-478 in a STZ-induced diabetic immunosuppressed mouse transplanted with human islets [a "humanized" diabetic mouse model (*14*)] could be performed to establish the relevance of PX-478 treatment to human β cell function in diabetes.

HIF-1α has been recognized as an important cancer drug target (*66*). Hence, the HIF-1α inhibitor PX-478 was originally developed for cancer therapy and has been tested in clinical trials in patients with advanced solid tumors (*67*, *68*). In the present study, we evaluated the potential of PX-478 as a new therapeutic agent to treat diabetes. Although the db/db mouse is a model with an extreme phenotype of type 2 diabetes, it has been widely used in the evaluation of antidiabetic compounds and is considered a mainstream strain for pharmaceutical efficacy testing (*69*). To acquire further mechanistic insights into PX-478 action, we complemented our studies using STZ mice, a model without insulin resistance, and could thereby demonstrate that PX-478 has a direct beneficial effect on β cell function. This suggests that PX-478 can serve as a promising glucose-lowering therapeutic strategy to preserve β cell function in diabetes.

MATERIALS AND METHODS

Study design

This study aimed to investigate the hypothesis that, in diabetes, cellular hypoxia contributes to β cell dysfunction and to assess the relevance of the PX-478 HIF-1α inhibitor as a new therapeutic approach to treat diabetes. We have performed several experiments using different approaches to address these objectives. The presence of HIF-1α protein in islets of diabetic mouse models was investigated using immunocytochemistry. The impact of high glucose metabolism on cellular hypoxia and HIF-1α–dependent pathway was studied using the hypoxia marker pimonidazole and performing Western blots and quantitative real-time polymerase chain reaction (qRT-PCR). The relevance of the HIF-1α inhibitor PX-478 treatment for the function of mouse pancreatic islets under high glucose metabolism was assessed by measuring insulin release and intracellular Ca^{2+} handling in the presence or absence of PX-478. The potential of PX-478 as a therapeutic agent to treat diabetes was examined by treating diabetic mouse models with the small-molecule HIF-1α inhibitor and by characterizing the metabolic state of the animals. Animals were randomly assigned to study groups. Experimenters were not blinded during the study.

Mouse models

All mice were housed in a temperature- and humidity-controlled room with 12-hour light/12-hour dark cycles with food and water ad libitum. All experiments were performed following Karolinska Institutet's guidelines for care and use of animals in research and reported following the Animal Research Reporting of In Vivo Experiments (ARRIVE) guidelines for animal studies. All procedures were approved by the Animal Review Board at the Court of Appeal of Northern Stockholm, under ethical permit numbers N99/12, N445/12, N144/14, 19462/2017, and 8822-2020. C57BL/6J mice as well as BKS.Cg-Dock7^{m} +/+ Lepr^{db}/J (db/db) mice and their normoglycemic heterozygous controls (db/+) were purchased from Charles River Laboratories (Germany and Italy, respectively). Db/db and db/+ mice of 12 weeks of age were used for immunocytochemistry. For in vitro studies, islets were isolated from C57BL/6J male mice at 3 to 5 months of age. C57BL/6J mice were fed with HFD (60 kcal % fat; D12492, Research Diets) for 12 weeks or 1 year before in vivo experiments with pimonidazole or immunohistochemistry of the pancreas, respectively. Glucose tolerance of HFD-fed mice used in pimonidazole experiments was assessed 2 weeks before the experiments, and animals displaying the highest levels of intolerance were selected. Leptin-deficient ob/ob mice used in the experiments originated from Umeå, Sweden and were inbred in the animal core facility at Karolinska Hospital. Discrimination from control lean littermates was achieved by phenotypic and genotypic analysis (*70*). Ob/ob mice used in the experiments were 10 to 14 weeks old and presented nonfasting hyperglycemia (above 15 mM glucose). C57BL/6J mice were rendered diabetic by administration of STZ (Sigma-Aldrich). Fourteen-week-old C57BL/6J mice received a daily dose of 50 mg of STZ per kilogram of body weight administered by intraperitoneal injection for five consecutive days. Blood glucose and body weight were monitored daily after the first STZ intraperitoneal injection. Blood glucose concentrations in mice were obtained using Accu-Chek Aviva monitoring system (Roche), which allows readings up to a maximum of 34.0 mM glucose. Higher values were considered 34.0 mM. Plasma insulin was measured by collecting blood from the mouse tail into EDTA-coated microcuvettes after centrifugation. Insulin was measured by AlphaLISA immunoassay (PerkinElmer) according to the manufacturer's instructions. Blood samples for measurement of glucose and insulin levels were acquired at the same time of day for the different experimental groups. HbA1c concentrations were assessed following the manufacturer's instructions using a DCA Vantage analyzer from Siemens.

Therapeutic treatment of mouse models

For experiments with pimonidazole (Hypoxyprobe, HPI Inc.), ob/ob mice or C57BL/6J mice fed with HFD and their nondiabetic controls were fasted for 10 to 12 hours before intraperitoneal injection of glucose at a dose of 2 g/kg body weight or saline solution. Fifteen minutes later, pimonidazole in a dose of 60 mg/kg body weight was delivered by intraperitoneal injection, and animals were sacrificed 1 hour 30 min later. Islets were isolated and immediately lysed. Blood glucose was measured at fixed time points during the experiment.

For experiments with the HIF-1α inhibitor PX-478 (Cayman Chemical Company), 6-week-old db/db mice were treated twice a week up to the age of 12 weeks. The mice were fed with wet food (chow) 2 hours before treatment. A solution of PX-478 in PBS (pH 7 to 7.4) was delivered by intraperitoneal injection at a dose of 30 mg/kg body weight (6 to 8 weeks of age) or 40 mg/kg body weight (9 to 12 weeks of age). Db/db mice (n = 9) received the intraperitoneal injection during a 30-min period after PX-478 solution was prepared. Db/+ mice (n = 5) and nontreated db/db mice (n = 10) received PBS. The db/db groups were organized randomly with each cage of animals containing some PX-478–treated and PBS-administered

mice. Mice treated with STZ that presented blood glucose values between 15 and 25 mM during two consecutive days were selected for the study with PX-478. STZ-induced diabetic mice were treated with PX-478 at a dose of 40 mg/kg body weight ($n = 6$) or with PBS ($n = 6$). C57BL/6J mice ($n = 7$) were used as controls for STZ-induced diabetic mice that were injected with PBS. The STZ groups were organized randomly with each cage of animals containing some PX-478–treated and PBS-administered mice. Gene expression analysis was performed in islets isolated from all PX-478–treated mice that showed blood glucose concentrations below 15 mM ($n = 5$) during the last week of intervention. Twelve-week-old C57BL/6J mice that were fed for 4 weeks with HFD were treated with a dose of 45 mg/kg ($n = 5$) or 30 mg/kg ($n = 6$) of PX-478 or PBS ($n = 6$). Lean control mice ($n = 6$) were also injected with PBS. HFD experimental groups were randomized, with each cage of animals containing mice from each group. Preparation of the PX-478 solution for STZ-induced diabetic and HFD-fed mice was done as described for db/db mice.

Statistical analysis

Statistical analysis was performed using GraphPad Prism 8.2.1 software. All results are based on biological replicates and presented as means ± SEM. Data normality was assessed using Shapiro-Wilk test. Significant differences between two groups were assessed with Student's *t* test. Analysis of variance (ANOVA) was used to assess statistical differences between more than two groups. The multiple comparisons tests used for analysis are specified in figure legends. Statistical significance was defined by $P < 0.05$. Statistical significances indicated by asterisks not associated with brackets represent analyses performed between treated islets and control untreated islets or between diabetic mouse models and their corresponding control animals, unless otherwise specified in figure legends.

SUPPLEMENTARY MATERIALS

www.science.org/doi/10.1126/scitranslmed.aba9112
Materials and Methods
Figs. S1 to S12
Tables S1 to S3
Data file S1
MDAR Reproducibility Checklist
References (*71*–*74*)

View/request a protocol for this paper from *Bio-protocol*.

REFERENCES AND NOTES

1. R. A. DeFronzo, M. A. Abdul-Ghani, Preservation of β-cell function: The key to diabetes prevention. *J. Clin. Endocrinol. Metab.* **96**, 2354–2366 (2011).
2. U.K. Prospective Diabetes Study Group, U.K. prospective diabetes study 16. Overview of 6 years' therapy of type II diabetes: A progressive disease. *Diabetes* **44**, 1249–1258 (1995).
3. D. R. Matthews, C. A. Cull, I. M. Stratton, R. R. Holman, R. C. Turner, UKPDS 26: Sulphonylurea failure in non-insulin-dependent diabetic patients over six years. UK Prospective Diabetes Study (UKPDS) Group. *Diabet. Med.* **15**, 297–303 (1998).
4. Y. Saisho, K. Kou, K. Tanaka, T. Abe, A. Shimada, T. Kawai, H. Itoh, Association between beta cell function and future glycemic control in patients with type 2 diabetes. *Endocr. J.* **60**, 517–523 (2013).
5. TODAY Study Group, Effects of metformin, metformin plus rosiglitazone, and metformin plus lifestyle on insulin sensitivity and β-cell function in TODAY. *Diabetes Care* **36**, 1749–1757 (2013).
6. J. D. Bagdade, E. L. Bierman, D. Porte Jr., The significance of basal insulin levels in the evaluation of the insulin response to glucose in diabetic and nondiabetic subjects. *J. Clin. Invest.* **46**, 1549–1557 (1967).
7. J. Erdmann, K. Pohnl, M. Mayr, O. Sypchenko, A. Naumann, S. Wagenpfeil, V. Schusdziarra, Disturbances of basal and postprandial insulin secretion and clearance in obese patients with type 2 diabetes mellitus. *Horm. Metab. Res.* **44**, 60–69 (2012).
8. B. C. Hansen, N. L. Bodkin, Beta-cell hyperresponsiveness: Earliest event in development of diabetes in monkeys. *Am. J. Physiol.* **259**, R612–R617 (1990).
9. B. C. Hansen, J. S. Striffler, N. L. Bodkin, Decreased hepatic insulin extraction precedes overt noninsulin dependent (type II) diabetes in obese monkeys. *Obes. Res.* **1**, 252–260 (1993).
10. M. B. Hoppa, S. Collins, R. Ramracheya, L. Hodson, S. Amisten, Q. Zhang, P. Johnson, F. M. Ashcroft, P. Rorsman, Chronic palmitate exposure inhibits insulin secretion by dissociation of Ca(2+) channels from secretory granules. *Cell Metab.* **10**, 455–465 (2009).
11. V. Nagaraj, A. S. Kazim, J. Helgeson, C. Lewold, S. Barik, P. Buda, T. M. Reinbothe, S. Wennmalm, E. Zhang, E. Renstrom, Elevated basal insulin secretion in type 2 diabetes caused by reduced plasma membrane cholesterol. *Mol. Endocrinol.* **30**, 1059–1069 (2016).
12. B. B. Boland, C. J. Rhodes, J. S. Grimsby, The dynamic plasticity of insulin production in β-cells. *Mol. Metab.* **6**, 958–973 (2017).
13. V. A. Salunkhe, R. Veluthakal, S. E. Kahn, D. C. Thurmond, Novel approaches to restore beta cell function in prediabetes and type 2 diabetes. *Diabetologia* **61**, 1895–1901 (2018).
14. M. H. Abdulreda, R. Rodriguez-Diaz, A. Caicedo, P. O. Berggren, Liraglutide compromises pancreatic β cell function in a humanized mouse model. *Cell Metab.* **23**, 541–546 (2016).
15. Y. Sato, H. Endo, H. Okuyama, T. Takeda, H. Iwahashi, A. Imagawa, K. Yamagata, I. Shimomura, M. Inoue, Cellular hypoxia of pancreatic beta-cells due to high levels of oxygen consumption for insulin secretion in vitro. *J. Biol. Chem.* **286**, 12524–12532 (2011).
16. M. Bensellam, B. Duvillie, G. Rybachuk, D. R. Laybutt, C. Magnan, Y. Guiot, J. Pouyssegur, J. C. Jonas, Glucose-induced O_2 consumption activates hypoxia inducible factors 1 and 2 in rat insulin-secreting pancreatic beta-cells. *PLOS ONE* **7**, e29807 (2012).
17. G. L. Semenza, Hypoxia-inducible factors: Mediators of cancer progression and targets for cancer therapy. *Trends Pharmacol. Sci.* **33**, 207–214 (2012).
18. K. Tanimoto, Y. Makino, T. Pereira, L. Poellinger, Mechanism of regulation of the hypoxia-inducible factor-1 alpha by the von Hippel-Lindau tumor suppressor protein. *EMBO J.* **19**, 4298–4309 (2000).
19. M. E. Cockman, N. Masson, D. R. Mole, P. Jaakkola, G. W. Chang, S. C. Clifford, E. R. Maher, C. W. Pugh, P. J. Ratcliffe, P. H. Maxwell, Hypoxia inducible factor-alpha binding and ubiquitylation by the von Hippel-Lindau tumor suppressor protein. *J. Biol. Chem.* **275**, 25733–25741 (2000).
20. T. Pereira, X. Zheng, J. L. Ruas, K. Tanimoto, L. Poellinger, Identification of residues critical for regulation of protein stability and the transactivation function of the hypoxia-inducible factor-1α by the von Hippel-Lindau tumor suppressor gene product. *J. Biol. Chem.* **278**, 6816–6823 (2003).
21. A. C. Epstein, J. M. Gleadle, L. A. McNeill, K. S. Hewitson, J. O'Rourke, D. R. Mole, M. Mukherji, E. Metzen, M. I. Wilson, A. Dhanda, Y. M. Tian, N. Masson, D. L. Hamilton, P. Jaakkola, R. Barstead, J. Hodgkin, P. H. Maxwell, C. W. Pugh, C. J. Schofield, P. J. Ratcliffe, C. elegans EGL-9 and mammalian homologs define a family of dioxygenases that regulate HIF by prolyl hydroxylation. *Cell* **107**, 43–54 (2001).
22. M. Ivan, K. Kondo, H. Yang, W. Kim, J. Valiando, M. Ohh, A. Salic, J. M. Asara, W. S. Lane, W. G. Kaelin Jr., HIFalpha targeted for VHL-mediated destruction by proline hydroxylation: Implications for O2 sensing. *Science* **292**, 464–468 (2001).
23. J. Zehetner, C. Danzer, S. Collins, K. Eckhardt, P. A. Gerber, P. Ballschmieter, J. Galvanovskis, K. Shimomura, F. M. Ashcroft, B. Thorens, P. Rorsman, W. Krek, PVHL is a regulator of glucose metabolism and insulin secretion in pancreatic beta cells. *Genes Dev.* **22**, 3135–3146 (2008).
24. V. H. Haase, J. N. Glickman, M. Socolovsky, R. Jaenisch, Vascular tumors in livers with targeted inactivation of the von Hippel-Lindau tumor suppressor. *Proc. Natl. Acad. Sci. U.S.A.* **98**, 1583–1588 (2001).
25. M. Y. Koh, T. Spivak-Kroizman, S. Venturini, S. Welsh, R. R. Williams, D. L. Kirkpatrick, G. Powis, Molecular mechanisms for the activity of PX-478, an antitumor inhibitor of the hypoxia-inducible factor-1alpha. *Mol. Cancer Ther.* **7**, 90–100 (2008).
26. G. E. Arteel, R. G. Thurman, J. A. Raleigh, Reductive metabolism of the hypoxia marker pimonidazole is regulated by oxygen tension independent of the pyridine nucleotide redox state. *Eur. J. Biochem.* **253**, 743–750 (1998).
27. X. Zheng, X. Zheng, X. Wang, Z. Ma, V. Gupta Sunkari, I. Botusan, T. Takeda, A. Bjorklund, M. Inoue, S. B. Catrina, K. Brismar, L. Poellinger, T. S. Pereira, Acute hypoxia induces apoptosis of pancreatic β-cell by activation of the unfolded protein response and upregulation of CHOP. *Cell Death Dis.* **3**, e322 (2012).
28. F. M. Matschinsky, A. K. Ghosh, M. D. Meglasson, M. Prentki, V. June, D. von Allman, Metabolic concomitants in pure, pancreatic beta cells during glucose-stimulated insulin secretion. *J. Biol. Chem.* **261**, 14057–14061 (1986).
29. W. J. Malaisse, A. C. Boschero, Calcium antagonists and islet function. XI. Effect of nifedipine. *Horm. Res.* **8**, 203–209 (1977).
30. J. C. Henquin, M. A. Ravier, M. Nenquin, J. C. Jonas, P. Gilon, Hierarchy of the beta-cell signals controlling insulin secretion. *Eur. J. Clin. Invest.* **33**, 742–750 (2003).
31. M. J. Merrins, C. Poudel, J. P. McKenna, J. Ha, A. Sherman, R. Bertram, L. S. Satin, Phase analysis of metabolic oscillations and membrane potential in pancreatic islet β-cells. *Biophys. J.* **110**, 691–699 (2016).

32. J. J. Brunt, S. Y. Shi, S. A. Schroer, T. Sivasubramaniyam, E. P. Cai, M. Woo, Overexpression of HIF-2α in pancreatic β cells does not alter glucose homeostasis. *Islets* **6**, e1006075 (2014).
33. R. Puff, P. Dames, M. Weise, B. Goke, J. Seissler, K. G. Parhofer, A. Lechner, Reduced proliferation and a high apoptotic frequency of pancreatic beta cells contribute to genetically-determined diabetes susceptibility of db/db BKS mice. *Horm. Metab. Res.* **43**, 306–311 (2011).
34. B. M. Wyse, W. E. Dulin, The influence of age and dietary conditions on diabetes in the db mouse. *Diabetologia* **6**, 268–273 (1970).
35. K. L. Corbin, C. D. Waters, B. K. Shaffer, G. M. Verrilli, C. S. Nunemaker, Islet hypersensitivity to glucose is associated with disrupted oscillations and increased impact of proinflammatory cytokines in islets from diabetes-prone male mice. *Endocrinology* **157**, 1826–1838 (2016).
36. C. Alarcon, B. B. Boland, Y. Uchizono, P. C. Moore, B. Peterson, S. Rajan, O. S. Rhodes, A. B. Noske, L. Haataja, P. Arvan, B. J. Marsh, J. Austin, C. J. Rhodes, Pancreatic β-cell adaptive plasticity in obesity increases insulin production but adversely affects secretory function. *Diabetes* **65**, 438–450 (2016).
37. Y. A. Moon, G. Liang, X. Xie, M. Frank-Kamenetsky, K. Fitzgerald, V. Koteliansky, M. S. Brown, J. L. Goldstein, J. D. Horton, The Scap/SREBP pathway is essential for developing diabetic fatty liver and carbohydrate-induced hypertriglyceridemia in animals. *Cell Metab.* **15**, 240–246 (2012).
38. V. Bonnevie-Nielsen, M. W. Steffes, A. Lernmark, A major loss in islet mass and B-cell function precedes hyperglycemia in mice given multiple low doses of streptozotocin. *Diabetes* **30**, 424–429 (1981).
39. M. Hahn, P. P. van Krieken, C. Nord, T. Alanentalo, F. Morini, Y. Xiong, M. Eriksson, J. Mayer, E. Kostromina, J. L. Ruas, J. Sharpe, T. Pereira, P. O. Berggren, E. Ilegems, U. Ahlgren, Topologically selective islet vulnerability and self-sustained downregulation of markers for β-cell maturity in streptozotocin-induced diabetes. *Commun. Biol.* **3**, 541 (2020).
40. A. A. Aughsteen, An ultrastructural study on the effect of streptozotocin on the islets of Langerhans in mice. *J. Electron Microsc. (Tokyo)* **49**, 681–690 (2000).
41. D. L. Eizirik, G. S. Korbutt, C. Hellerstrom, Prolonged exposure of human pancreatic islets to high glucose concentrations in vitro impairs the beta-cell function. *J. Clin. Invest.* **90**, 1263–1268 (1992).
42. J. Mir-Coll, T. Moede, M. Paschen, A. Neelakandhan, I. Valladolid-Acebes, B. Leibiger, A. Biernath, C. Ammala, I. B. Leibiger, B. Yesildag, P. O. Berggren, Human islet microtissues as an in vitro and an in vivo model system for diabetes. *Int. J. Mol. Sci.* **22**, (2021).
43. E. Lorza-Gil, F. Gerst, M. B. Oquendo, U. Deschl, H. U. Haring, M. Beilmann, S. Ullrich, Glucose, adrenaline and palmitate antagonistically regulate insulin and glucagon secretion in human pseudoislets. *Sci. Rep.* **9**, 10261 (2019).
44. D. Zhang, Y. Liu, Y. Tang, X. Wang, Z. Li, R. Li, Z. Ti, W. Gao, J. Bai, Y. Lv, Increased mitochondrial fission is critical for hypoxia-induced pancreatic beta cell death. *PLOS ONE* **13**, e0197266 (2018).
45. S. Puri, D. A. Cano, M. Hebrok, A role for von Hippel-Lindau protein in pancreatic beta-cell function. *Diabetes* **58**, 433–441 (2009).
46. J. Cantley, C. Selman, D. Shukla, A. Y. Abramov, F. Forstreuter, M. A. Esteban, M. Claret, S. J. Lingard, M. Clements, S. K. Harten, H. Asare-Anane, R. L. Batterham, P. L. Herrera, S. J. Persaud, M. R. Duchen, P. H. Maxwell, D. J. Withers, Deletion of the von Hippel-Lindau gene in pancreatic β cells impairs glucose homeostasis in mice. *J. Clin. Invest.* **119**, 125–135 (2009).
47. K. Cheng, K. Ho, R. Stokes, C. Scott, S. M. Lau, W. J. Hawthorne, P. J. O'Connell, T. Loudovaris, T. W. Kay, R. N. Kulkarni, T. Okada, X. L. Wang, S. H. Yim, Y. Shah, S. T. Grey, A. V. Biankin, J. G. Kench, D. R. Laybutt, F. J. Gonzalez, C. R. Kahn, J. E. Gunton, Hypoxia-inducible factor-1α regulates β cell function in mouse and human islets. *J. Clin. Invest.* **120**, 2171–2183 (2010).
48. J. E. Gunton, R. N. Kulkarni, S. Yim, T. Okada, W. J. Hawthorne, Y.-H. Tseng, R. S. Roberson, C. Ricordi, P. J. O'Connell, F. J. Gonzalez, C. R. Kahn, Loss of *ARNT/HIF1*β mediates altered gene expression and pancreatic-islet dysfunction in human type 2 diabetes. *Cell* **122**, 337–349 (2005).
49. M. Hoang, S. Paglialunga, E. Bombardier, A. R. Tupling, J. W. Joseph, The loss of ARNT/HIF1β in male pancreatic β-cells is protective against high-fat diet-induced diabetes. *Endocrinology* **160**, 2825–2836 (2019).
50. L. B. Tanner, A. G. Goglia, M. H. Wei, T. Sehgal, L. R. Parsons, J. O. Park, E. White, J. E. Toettcher, J. D. Rabinowitz, Four key steps control glycolytic flux in mammalian cells. *Cell Syst* **7**, 49–62.e8 (2018).
51. H. Ishihara, T. Asano, K. Tsukuda, H. Katagiri, K. Inukai, M. Anai, M. Kikuchi, Y. Yazaki, J. Miyazaki, Y. Oka, Overexpression of hexokinase I but not GLUT1 glucose transporter alters concentration dependence of glucose-stimulated insulin secretion in pancreatic beta-cell line MIN6. *J. Biol. Chem.* **269**, 3081–3087 (1994).
52. G. W. Gould, G. D. Holman, The glucose transporter family: Structure, function and tissue-specific expression. *Biochem. J* **295** (Pt. 2), 329–341 (1993).
53. E. Glynn, B. Thompson, S. Vadrevu, S. Lu, R. T. Kennedy, J. Ha, A. Sherman, L. S. Satin, Chronic glucose exposure systematically shifts the oscillatory threshold of mouse islets: Experimental evidence for an early intrinsic mechanism of compensation for hyperglycemia. *Endocrinology* **157**, 611–623 (2016).
54. Z. Li, F. A. Karlsson, S. Sandler, Islet loss and alpha cell expansion in type 1 diabetes induced by multiple low-dose streptozotocin administration in mice. *J. Endocrinol.* **165**, 93–99 (2000).
55. T. Takasu, S. Takakura, Protective effect of ipragliflozin on pancreatic islet cells in obese type 2 diabetic db/db mice. *Biol. Pharm. Bull.* **41**, 761–769 (2018).
56. T. Kimura, A. Obata, M. Shimoda, S. Okauchi, Y. Kanda-Kimura, Y. Nogami, S. Moriuchi, H. Hirukawa, K. Kohara, S. Nakanishi, T. Mune, K. Kaku, H. Kaneto, Protective effects of the SGLT2 inhibitor luseogliflozin on pancreatic β-cells in db/db mice: The earlier and longer, the better. *Diabetes Obes. Metab.* **20**, 2442–2457 (2018).
57. B. B. Boland, C. Brown Jr., M. L. Boland, J. Cann, M. Sulikowski, G. Hansen, R. V. Grønlund, W. King, C. Rondinone, J. Trevaskis, C. J. Rhodes, J. S. Grimsby, Pancreatic β-cell rest replenishes insulin secretory capacity and attenuates diabetes in an extreme model of obese type 2 diabetes. *Diabetes* **68**, 131–140 (2019).
58. A. Kanno, S. I. Asahara, M. Kawamura, A. Furubayashi, S. Tsuchiya, E. Suzuki, T. Takai, M. Koyanagi-Kimura, T. Matsuda, Y. Okada, W. Ogawa, Y. Kido, Early administration of dapagliflozin preserves pancreatic β-cell mass through a legacy effect in a mouse model of type 2 diabetes. *J Diabetes Investig.* **10**, 577–590 (2019).
59. C. Jiang, A. Qu, T. Matsubara, T. Chanturiya, W. Jou, O. Gavrilova, Y. M. Shah, F. J. Gonzalez, Disruption of hypoxia-inducible factor 1 in adipocytes improves insulin sensitivity and decreases adiposity in high-fat diet-fed mice. *Diabetes* **60**, 2484–2495 (2011).
60. K. Sun, N. Halberg, M. Khan, U. J. Magalang, P. E. Scherer, Selective inhibition of hypoxia-inducible factor 1α ameliorates adipose tissue dysfunction. *Mol. Cell. Biol.* **33**, 904–917 (2013).
61. C. Jiang, J. H. Kim, F. Li, A. Qu, O. Gavrilova, Y. M. Shah, F. J. Gonzalez, Hypoxia-inducible factor 1α regulates a SOCS3-STAT3-adiponectin signal transduction pathway in adipocytes. *J. Biol. Chem.* **288**, 3844–3857 (2013).
62. E. Ferrannini, A. Gastaldelli, Y. Miyazaki, M. Matsuda, A. Mari, R. A. DeFronzo, β-cell function in subjects spanning the range from normal glucose tolerance to overt diabetes: A new analysis. *J Clin. Endocrinol. Metab.* **90**, 493–500 (2005).
63. C. M. Cohrs, J. K. Panzer, D. M. Drotar, S. J. Enos, N. Kipke, C. Chen, R. Bozsak, E. Schoniger, F. Ehehalt, M. Distler, A. Brennand, S. R. Bornstein, J. Weitz, M. Solimena, S. Speier, Dysfunction of persisting β cells is a key feature of early type 2 diabetes pathogenesis. *Cell Rep.* **31**, 107469 (2020).
64. M. Nagao, J. L. S. Esguerra, A. Asai, J. K. Ofori, A. Edlund, A. Wendt, H. Sugihara, C. B. Wollheim, S. Oikawa, L. Eliasson, Potential protection against type 2 diabetes in obesity through lower CD36 expression and improved exocytosis in β-cells. *Diabetes* **69**, 1193–1205 (2020).
65. I. Matsumoto, T. Sawada, M. Nakano, T. Sakai, B. Liu, J. D. Ansite, H.-J. Zhang, R. Kandaswamy, D. E. R. Sutherland, B. J. Hering, Improvement in islet yield from obese donors for human islet transplants. *Transplantation* **78**, 880–885 (2004).
66. L. Schito, G. L. Semenza, Hypoxia-inducible factors: Master regulators of cancer progression. *Trends Cancer* **2**, 758–770 (2016).
67. R. Tibes, G. S. Falchook, D. D. Von Hoff, G. J. Weiss, T. Iyengar, R. Kurzrock, L. Pestano, A. M. Lowe, R. S. Herbst, Results from a phase I, dose-escalation study of PX-478, an orally available inhibitor of HIF-1α. *J Clin. Onc.* **28**, 3076–3076 (2010).
68. S. Welsh, R. Williams, L. Kirkpatrick, G. Paine-Murrieta, G. Powis, Antitumor activity and pharmacodynamic properties of PX-478, an inhibitor of hypoxia-inducible factor-1α. *Mol. Cancer Ther.* **3**, 233–244 (2004).
69. E. H. Leiter, M. Strobel, A. O'Neill, D. Schultz, A. Schile, P. C. Reifsnyder, Comparison of two new mouse models of polygenic type 2 diabetes at the jackson laboratory, NONcNZO10Lt/J and TALLYHO/JngJ. *J. Diabetes Res.* **2013**, 165327 (2013).
70. J. D. Ellett, Z. P. Evans, G. Zhang, K. D. Chavin, D. D. Spyropoulos, A rapid PCR-based method for the identification of ob mutant mice. *Obesity* **17**, 402–404 (2009).
71. D. E. Richard, E. Berra, E. Gothie, D. Roux, J. Pouyssegur, p42/p44 mitogen-activated protein kinases phosphorylate hypoxia-inducible factor 1α (HIF-1α) and enhance the transcriptional activity of HIF-1. *J. Biol. Chem.* **274**, 32631–32637 (1999).
72. S. Picelli, O. R. Faridani, A. K. Bjorklund, G. Winberg, S. Sagasser, R. Sandberg, Full-length RNA-seq from single cells using Smart-seq2. *Nat. Protoc.* **9**, 171–181 (2014).
73. P. P. van Krieken, A. Voznesenskaya, A. Dicker, Y. Xiong, J. H. Park, J. I. Lee, E. Ilegems, P. O. Berggren, Translational assessment of a genetic engineering methodology to improve islet function for transplantation. *EBioMedicine* **45**, 529–541 (2019).
74. E. Ilegems, P. P. van Krieken, P. K. Edlund, A. Dicker, T. Alanentalo, M. Eriksson, S. Mandic, U. Ahlgren, P. O. Berggren, Light scattering as an intrinsic indicator for pancreatic islet cell mass and secretion. *Sci. Rep.* **5**, 10740 (2015).

Acknowledgments: We thank Xiaowei Zheng for providing primers for gene expression analysis. **Funding**: This work was supported by funding from Karolinska Institutet (to E.I.), the Strategic Research Program in Diabetes at Karolinska Institutet (to P.-O.B. and J.L.R.), the Swedish Research Council (to P.-O.B. and J.L.R.), the Novo Nordisk Foundation (to P.-O.B. and

J.L.R.), the Swedish Diabetes Association (to P.-O.B.), the Family Knut and Alice Wallenberg Foundation (to P.-O.B.), Diabetes Research and Wellness Foundation (to P.-O.B.), the Jonas & Christina af Jochnick Foundation (to P.-O.B.), the Family Erling-Persson Foundation (to P.-O.B.), Berth von Kantzow's Foundation (to P.-O.B.), the Skandia Insurance Company Ltd. (to P.-O.B.), European Research Council grant ERC-2018-AdG 834860 EYELETS (to P.-O.B.), the European Union's Seventh Framework Programme under grant agreement nos. 289932 and 613879 (to P.-O.B.), and the European Diabetes Research Programme in Cellular Plasticity Underlying the Pathophysiology of Type 2 Diabetes (to T.S.P. and E.I.). **Author contributions**: T.S.P. and P.-O.B. supervised the study. T.S.P. conceived, coordinated, and designed the study. E.I., T.S.P., G.B., and J.C. performed and analyzed experiments. E.B. provided reagents. B.Y. provided human islet organoids. T.S.P., E.I., and J.L.R. wrote the manuscript. P.-O.B. revised and edited the manuscript. All authors reviewed the results and approved the final version of the manuscript. **Competing interests**: P.-O.B. is the founder and CEO of Biocrine AB. E.I. is a consultant for Biocrine AB. B.Y. is an employee at InSphero AG. T.S.P. has filed a PCT patent titled "Treatment of diabetes" with the number WO 2020/224527 A1. All other authors declare that they have no competing financial interests. **Data and materials availability**: All data associated with this study are present in the paper or the Supplementary Materials. Raw data are available in data file S1.

Submitted 15 January 2020
Resubmitted 14 December 2021
Accepted 23 February 2022
Published 30 March 2022
10.1126/scitranslmed.aba9112

Science Translational Medicine

HIF-1# inhibitor PX-478 preserves pancreatic # cell function in diabetes

Erwin IlegemsGalyna BryzgalovaJorge CorreiaBurcak YesildagEdurne BerraJorge L. RuasTeresa S. PereiraPer-Olof Berggren

Sci. Transl. Med., 14 (638), eaba9112. • DOI: 10.1126/scitranslmed.aba9112

Inhibiting HIF-1# improves glucose homeostasis
Type 2 diabetes (T2D) places insulin-secreting beta cells under sustained metabolic stress. Ilegems *et al.* reasoned that such stress might result in a hypoxic state and thereby impair # cell function. The authors confirmed a glucose metabolism–mediated increase in hypoxia in multiple mouse models with metabolic dysfunction and showed that a HIF-1# inhibitor improved # cell function in db/db and streptozotocin-induced mouse models of diabetes. Human islet organoids cultured under high-glucose conditions also showed improved # cell function in response to HIF-1# inhibitor treatment, suggesting that these findings may translate to humans.

Science Translational Medicine
AAAS

Supplementary Materials for

HIF-1α inhibitor PX-478 preserves pancreatic β cell function in diabetes

Erwin Ilegems *et al.*

Corresponding author: Erwin Ilegems, erwin.ilegems@ki.se; Teresa S. Pereira, teresa.pereira@ki.se; Per-Olof Berggren, per-olof.berggren@ki.se

Sci. Transl. Med. **14**, eaba9112 (2022)
DOI: 10.1126/scitranslmed.aba9112

The PDF file includes:

Other Supplementary Material for this manuscript includes the following:

Materials and Methods

Islet isolation

Mice were sacrificed by cervical dislocation and their pancreata perfused with 3-5 ml of 1 mg/ml collagenase P (Roche) in Hank´s balance salt solution (HBSS) (Sigma) buffered with HEPES (pH 7.4) supplemented with 0.25% bovine serum albumin (BSA). Pancreata were thereafter extracted and digested in a water bath at 37 ˚C for 22-28 min. Islets were handpicked in ice-cold HBSS buffered with HEPES (pH 7.4) containing 0.5% BSA. Prior to in vitro experimentations islets were cultured overnight in RPMI 1640 medium supplemented with 10% fetal calf serum (FCS), L-glutamine (2 mM), penicillin (100 U/ml) and streptomycin (100 U/ml) (Life Technologies). Islets were kept at 37 ˚C in a humidified atmosphere with 5% CO_2. Islets of db/db and db/+ mice used to assess expression of proteins encoded by HIF-1α-target genes were lysed immediately after isolation. Islets from STZ-induced diabetic and corresponding controls were immediately either lysed or fixated after isolation.

Treatment of islets of Langerhans

For experiments using the hypoxic marker pimonidazole, mouse islets were cultured overnight in RPMI 1640 with 11 mM glucose and fasted for 1 hour in RPMI 1640 with 5.5 mM glucose. Subsequently islets were moved to medium containing 5.5 mM, 11 mM or 22 mM glucose, either with or without 10 μM of the glucokinase (GCK) activator GKA50 (Sigma), 50 μM nifedipine (Sigma) or 100 μM diazoxide (Sigma). Islets were treated during 2 or 8 hours before lysis. During the last 2 hours of culture, 200 μM pimonidazole was added to the medium. The hypoxic samples were cultured under 8% O_2 in the presence of 11 mM glucose during 2 hours before the lysis of the islets.

In the experiments performed with mouse islets to detect HIF-1α by Western blot analysis, assess HIF-1α target gene expression, measure release of insulin in static batch incubations or determine changes in cytoplasmic free Ca^{2+} concentration ($[Ca^{2+}]_i$), isolated islets were cultured for 18-24 hours in RPMI 1640 medium with 11 mM glucose and then fasted 1-2 hours at 5.5 mM glucose. Islets were then cultured at 11 mM of glucose with or without treatment with 50 μM of PX-478 and in the presence or absence of 20 μM of the GCK activator GKA50 (Sigma) or exposed to hypoxia. In static batch incubations a concentration of 10 μM of GKA50 was also tested. For Western blots of HIF-1α and GLUT1, insulin release and determination of $[Ca^{2+}]_i$, islets were

treated for a period of 20 hours, while for gene expression assays a 16 hours treatment was performed. For gene expression assays, islets were exposed to hypoxia for 8 hours. In experiments assessing protein abundance and gene expression assays, islet preparations of 3 mice were pulled together and groups of 100-120 islet/sample or 30-50 islet/sample were lysed in RIPA or RNA lysis buffer, respectively. An individual islet preparation derived from one mouse was used for each experiment assessing insulin release. Islets used to determine changes in $[Ca^{2+}]_i$ were obtained from 3 independent islet preparations.

Production and culture of human islet organoids

Human islet organoids were produced by InSphero (InSphero AG). Briefly, primary human islets (Prodo Laboratories Inc.) were dispersed, reaggregated using a multi-well hanging drop system, and transferred into Akura 96 plates (InSphero AG) for quality assessment (table S3). For each production lot, individual islet organoids are assessed for the characterization of size distribution, stimulation index (determined by measuring static insulin released during 2 hours in 50 µl Krebs-Ringer bicarbonate HEPES buffer containing either 2.8 mM or 16.7 mM glucose), and total ATP content (using CellTiter-Glo 3D Cell Viability Assay, Promega). After transportation, human islet organoids were hand-picked, transferred into suspension culture dishes containing 3D InSight Human Islet Maintenance Medium (InSphero AG) and kept at 37 ˚C in a humidified atmosphere with 5% CO_2. Twenty-four hours later, human islet organoids were placed into medium containing either 5.5 mM or 16.7 mM glucose and remained under these glucose concentrations during 15 days. At day 10 of culture, organoids were treated with 25 µM of PX-478 during 4 consecutive days.

Protein extraction and immunoblotting assays

Islets were sonicated in RIPA buffer (50 mM Tris-HCl pH 7.4, 150 mM NaCl, 1% NP-40, 0.5% Na deoxycholate, 0.1% SDS, 1 mM EDTA, protease inhibitor mix (Complete-Mini, Roche), 0.5 mM phenylmethylsulfonyl fluoride (PMSF) and 0.5 mM dithiothreitol). Lysates were cleared by centrifugation for 30 min at 15,000 g and proteins were separated by SDS-PAGE and blotted onto nitrocellulose membranes. Blocking was performed at room temperature for 2 hours in TBS buffer (50 mM Tris-HCl pH 7.4 and 150 mM NaCl) with 5% nonfat milk, followed by incubation with primary antibodies of anti-pimonidazole adducts (1:500, PAb2627(AP), Hypoxyprobe, HPI Inc.) or anti-HIF-1α (1:200, NB100-449, RRID:AB_10001045), anti-GLUT2 (1:5000, NBP2-22218,

RRID:AB_2335858), anti-G6PD (1:5000, NB100-236, RRID:AB_2107663), anti-LDHA (1:10,000, NBP1-48336, RRID:AB_10011099) (Novus Biologicals), anti-GLUT1 (1:100,000, ab115730, RRID:AB_10903230), anti-PDK1 (1:5000, ab202468), anti-β-Actin (1:5000, ab6278) (Abcam) and anti-Tubulin (1:1000, MAB11106, RRID:AB_2888691, Abnova) in TBS with 2% nonfat milk overnight at 4 ˚C. After several washes with TBS containing 0.5% Tween 20, the membranes were incubated with the secondary antibody anti-rabbit IgG/HRP (7074P2, RRID:AB_2099233, Cell Signaling Technology) or anti-mouse IgG/HRP (NA931, RRID:AB_772210, GE Healthcare) in TBS with 1% nonfat milk. Following several washes, proteins were visualized using chemiluminescence (GE Healthcare or Bio-Rad) according to the manufacturer´s instructions. As internal control for the calculation of protein levels, membranes were stained with Ponceau (Sigma) or ChemiDoc stain free imaging system (Bio-Rad). Protein bands were quantified using ImageJ (NIH).

Static batch incubation of mouse islets and human islet organoids

For measurements of insulin release from mouse islets, groups of 6 islets were first fasted for 2 hours at 37 ˚C in perifusion buffer (pH 7.4, containing 125 mM NaCl, 5.9 mM KCl, 2.6 mM $CaCl_2$, 1.2 mM $MgCl_2$, 25 mM HEPES, and 0.1% BSA) containing 3.3 mM glucose. After the first 2 hours of fasting, insulin release was measured from islets incubated for 1 hour at 3.3 mM glucose and subsequently 1 hour at 16.7 mM glucose. Due to the heterogeneous size of mouse islets, insulin release was normalized to DNA. For human islet organoids, groups of 4 islet organoids were fasted for 2 hours at 37 ˚C in perifusion buffer containing 2.8 mM glucose, followed by the measurement of insulin release after incubation for 1 hour at 2.8 mM glucose, and after subsequent incubation for 1 hour at 16.7 mM glucose. Considering the homogenous size of human islet organoids (table S3) and the lack of impact of PX-478 on islet DNA content (fig. S12), insulin release from human islet organoids was not normalized to DNA and is presented as insulin release per islet organoid. For the measurement of insulin content, islets were lysed in M-PER extraction buffer (Thermo Fisher Scientific). Insulin concentration was assessed by AlphaLISA (Perkin Elmer). DNA content was measured by QuantIT Picogreen dsDNA kit (Thermo Fisher Scientific).

Measurements of $[Ca^{2+}]_i$

Changes in $[Ca^{2+}]_i$ were recorded in islets treated with 20 μM GKA50 and co-treated with or without 50 μM PX-478. After 20 hours of treatment islets were fasted for 2 hours in perifusion

buffer with 3 mM glucose and during the last hour of fasting islets were loaded with 2 mM Fura-2AM (Thermo Fisher Scientific). Cytoplasmic free Ca^{2+} measurements were performed by attaching islets to a cover slip using PuraMatrix Hydrogel (BD Biosciences) and fluorescence was recorded using an inverted epifluorescence Axiovert 135 microscope (Zeiss) connected to a SPEX Industries Fluorolog spectrofluorometer for dual-wavelength excitation fluorimetry. Islets were perifused at 37 ˚C with buffer supplemented with either 3 mM glucose, 16.7 mM glucose or 3 mM glucose + 25 mM KCl, and simultaneously excited at 340 and 380 nm. Fluorescence emission was recorded and the ratio of intensities obtained by these two excitation wavelengths was calculated for normalization.

Glucose and insulin tolerance test

Mice were fasted for 6 hours prior to glucose tolerance tests (GTT) or insulin tolerance tests (ITT). For the GTT, mice received an IP injection of 1.5 g/kg body weight of glucose. For the ITT, mice received an IP injection of 0.5 U insulin/kg body weight (Actrapid Penfill). Blood glucose was measured at fixed time points up to 120 min or 180 min post injection, as indicated. HOMA-IR was calculated as fasting insulin (mU/L) x fasting glucose (mM)/22.5. HOMA-β was calculated as (fasting insulin (mU/L) x 20)/(fasting glucose (mM) - 3.5).

Frozen sections and immunocytochemistry

Anesthetized mice were perfused through the heart left ventricle with ice cold PBS supplemented with 3 IE/ml heparin and subsequently with ice cold 4% paraformaldehyde (PFA). The pancreas was removed and kept at 4 ˚C during 5 hours in PFA and was then moved to 30% sucrose. After staying in sucrose overnight at 4 ˚C it was frozen and maintained at -80 ˚C. Frozen pancreata were sectioned with 20 μm thickness. Sections were blocked in a TBS buffer containing 0.1% Triton X-100 and supplemented with 10% FBS. Primary antibodies rabbit anti-mouse HIF-1α antibody (1:100) (*71*), rat anti-mouse Ki67 antibody (1:100, SolA15, RRID:AB_10853185, Invitrogen), guinea pig anti-mouse insulin antibody (1:1000, A0564, RRID:AB_10013624, DAKO), mouse anti-glucagon (1:1000, G2654, RRID:AB_259852, Sigma) or rat anti-human somatostatin (1:700, 8330-0009, RRID:AB_2195908, Bio-Rad) and secondary antibodies goat anti-rabbit Alexa 488 (1:500, A11034, RRID:AB_2576217), goat anti-rat Alexa 546 (1:500, A11081, RRID:AB_141738) and goat anti-guinea pig Alexa 633 (1:500, A21105, RRID:AB_1500611) or goat anti-mouse Alexa 546 (1:500, A21123, RRID:AB_141592) (Thermo Fisher Scientific) were

incubated at 4 ˚C overnight in the buffer containing 0.1% Triton X-100. Frozen sections were further mounted with ProLong Gold Antifade with DAPI (Thermo Fisher Scientific). Images were acquired using a Leica SP5 system confocal microscope system (Leica Microsystems).

Whole mount staining

Islets were immediately fixed following isolation in 4% paraformaldehyde (PFA) for 1 hour on ice and washed with PBS. Samples were blocked for 3-4 hours in PBS containing 10% goat serum and 0.3% Triton-X100, and stained overnight with primary antibodies (guinea pig anti-insulin (1:1000, A0564, RRID:AB_10013624, DAKO), rabbit anti-glucagon (1:300, PU039-5UP, BioGenex), rat anti-somatostatin (1:500, 8330-0009, RRID:AB_2195908, Bio-Rad), dissolved in blocking buffer), and overnight with secondary antibodies (goat anti-guinea pig Alexa 488 (1:1000, A11073, RRID:AB_2534117, Thermo Fisher Scientific), goat anti-rabbit Alexa 633 (1:1000, A21071, RRID:AB_141419, Thermo Fisher Scientific) and goat anti-rat Alexa 546 (1:1000, A11081, RRID:AB_141738, Thermo Fisher Scientific), dissolved in blocking buffer). Whole mounts were imaged by confocal microscopy, using a Leica SP5 confocal microscope system (Leica Microsystems).

Transmission electron microscopy (TEM)

Isolated islets were fixed in 2.5% glutaraldehyde + 1% paraformaldehyde in 0.1 M phosphate buffer, pH 7.4. Specimens were rinsed in 0.1 M phosphate buffer, pH 7.4 and postfixed in 2% osmium tetroxide 0.1 M phosphate buffer, pH 7.4 at 4°C for two hours, stepwise dehydrated in ethanol followed by acetone and finally embedded in LX-112 (Ladd). Ultrathin sections (approximately 50–60 nm) were prepared using a Leica EM UC 7 ultramicrotome (Leica) and contrasted with uranyl acetate followed by lead citrate and examined in a Hitachi HT7700 transmission electron microscope (Hitachi Hightech) at 100 kV. Digital images were acquired using a Veleta camera (Olympus Soft Imaging Solutions, GmbH).

Gene expression analysis

For gene expression analysis of pancreatic islets, approximately 30-50 islets were collected and RNA was prepared using RNeasy Micro Kit (QIAGEN) following the manufacturer's instructions. Full-length cDNA was produced by reverse transcription using Superscript II (Thermo Fisher Scientific), amplified and purified as described previously (*72*). Quantitative RT-PCR was performed using SYBR Green (Thermo Fisher Scientific) and a QuantStudio 5 system (Thermo

Fisher Scientific). Concentrations of all samples were normalized prior to qRT-PCR experiments, all genes were normalized to porphobilinogen deaminase (*Pbgd*).

For gene expression analysis of liver and adipose tissue, total RNA was isolated from frozen tissues using the TRI Reagent (Sigma) according to the manufacturer´s instructions, DNase-treated, and reverse transcribed using the High Capacity RNA-to-cDNA Kit (Applied Biosystems). Gene expression was analyzed using Applied Biosystems' Power SYBR Green PCR Master Mix and ViiA 7 Real-Time PCR system. Gene expression was normalized to hypoxanthine phosphoribosyltransferase (*Hprt*) expression and expressed relative to experimental controls. Primer sequences are listed in table S1.

Image analysis

Image analysis protocols were established in Volocity (Perkin Elmer) for automated analysis of histological sections. In studies assessing proliferation rate the average β cell section area was obtained by dividing the insulin-stained area by the total number of DAPI-stained nuclei enclosed in this area (minimum of 1000 cells per tissue). β cell average area was used to calculate the number of β cells in islets of db/db pancreata. The β cell proliferation rate was calculated by counting Ki67-insulin positive nuclei and dividing by the total number of β cells of each islet. Quantification of whole mount stainings were performed on two optical sections per islet, as described previously (*73*). Backscatter signal (*74*) was used to delineate islet areas of each optical section. For electron microscopy image analysis, the opacity of insulin-containing granules was analyzed by manual selection of regions of interest in images obtained from n = 60 (control), 30 (STZ PBS) and 43 islets (STZ PX-478) isolated from 6, 4, and 5 mice respectively. Average pixel intensities were pooled per group from a total of 8217 granules, granule density was averaged per image (n=6, 7, and 5 images for control, STZ PBS and STZ PX-478 respectively). Volocity and ImageJ were used for image display.

Supplementary Figures

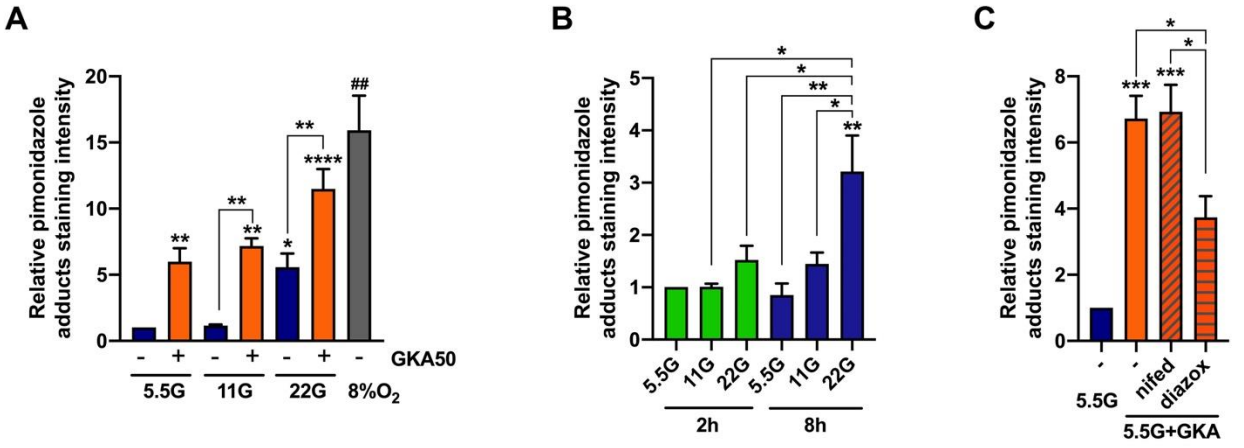

Fig. S1. Increased glucose metabolism in isolated C57BL/6J mouse islets leads to cellular hypoxia. (**A**), (**B**) and (**C**) correspond to quantifications of Fig. 2G, 2H and 2I, respectively. Each graphic represents three independent experiments. For each experiment islet preparations of 3 mice were pulled together. (A) Statistical significance associated with brackets indicate differences between islets treated with GKA50 and their corresponding controls. * $p<0.05$, ** $p<0.01$, *** $p<0.001$, **** $p<0.0001$ by two-way ANOVA with Tukey´s multiple comparisons test (A and B), by one-way ANOVA with Tukey´s multiple comparisons test (C). ## $p<0.01$ by two-tailed paired Student's t-test to compare values of 8% O_2 with untreated 5.5G.

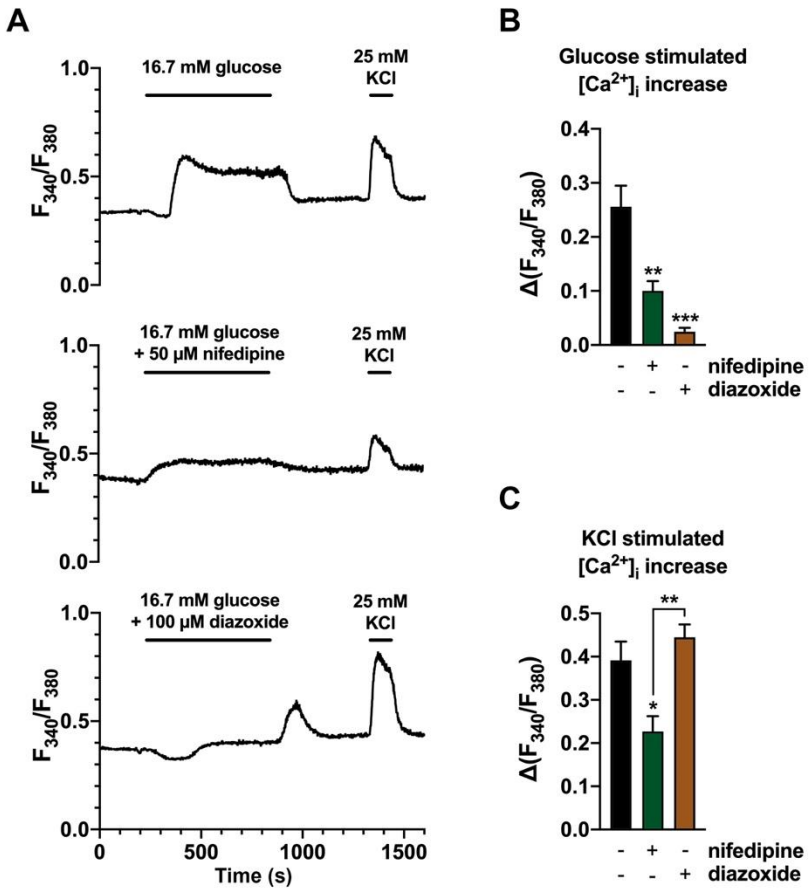

Fig. S2. Effects of nifedipine and diazoxide on intracellular Ca^{2+} handling in isolated C57BL/6J mouse islets. (**A**) Isolated islets were loaded with the fluorescent $[Ca^{2+}]_i$ indicator Fura-2 and incubated for 1 hour at 3 mM glucose concentration. Changes in $[Ca^{2+}]_i$ were recorded in response to an increase in glucose concentration and to KCl-induced plasma membrane depolarization. The presence in the high glucose-containing buffer of 50 µM nifedipine (middle trace) or 100 µM diazoxide (lower trace) affected intracellular Ca^{2+} handling by respectively inhibiting the opening of Ca^{2+} channels and activating K^+ channels. Quantitative analyses of the traces indicate (**B**) a reduction in $\Delta[Ca^{2+}]_i$ response amplitude to an increase in glucose concentration by simultaneous incubation with nifedipine or diazoxide, and (**C**) a blunted response to KCl subsequent to nifedipine administration. Traces are representative of $n \geq 4$ islets per condition. * $p<0.05$, ** $p<0.01$, *** $p<0.001$ by one-way ANOVA with Tukey's multiple comparisons test.

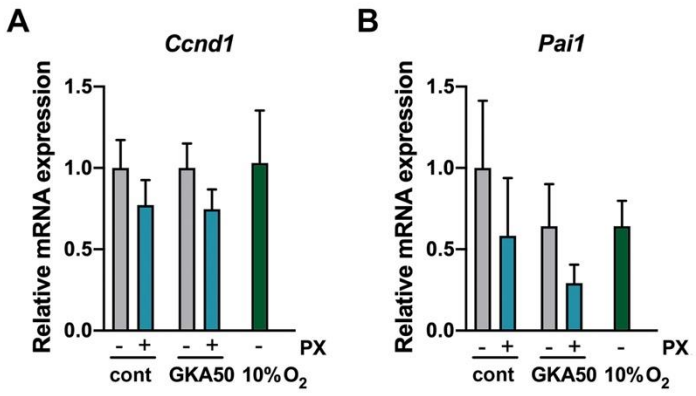

Fig. S3. Effect of increased GCK activity or exposure to hypoxia on the expression of HIF-2α target genes in isolated C57BL/6J mouse islets. Gene expression of HIF-2α-target genes (**A**) *Ccnd1* and (**B**) *Pai1*, analyzed by qRT-PCR. Islets were cultured in the presence (GKA50) or absence (cont) of the GCK activator for 16 hours or exposed to hypoxia (10% O_2) for 8 hours and treated with PX-478 (PX) as indicated. n=3-4 islet preparations per condition. No statistical significance was detected (two-way ANOVA with Tukey's multiple comparisons test).

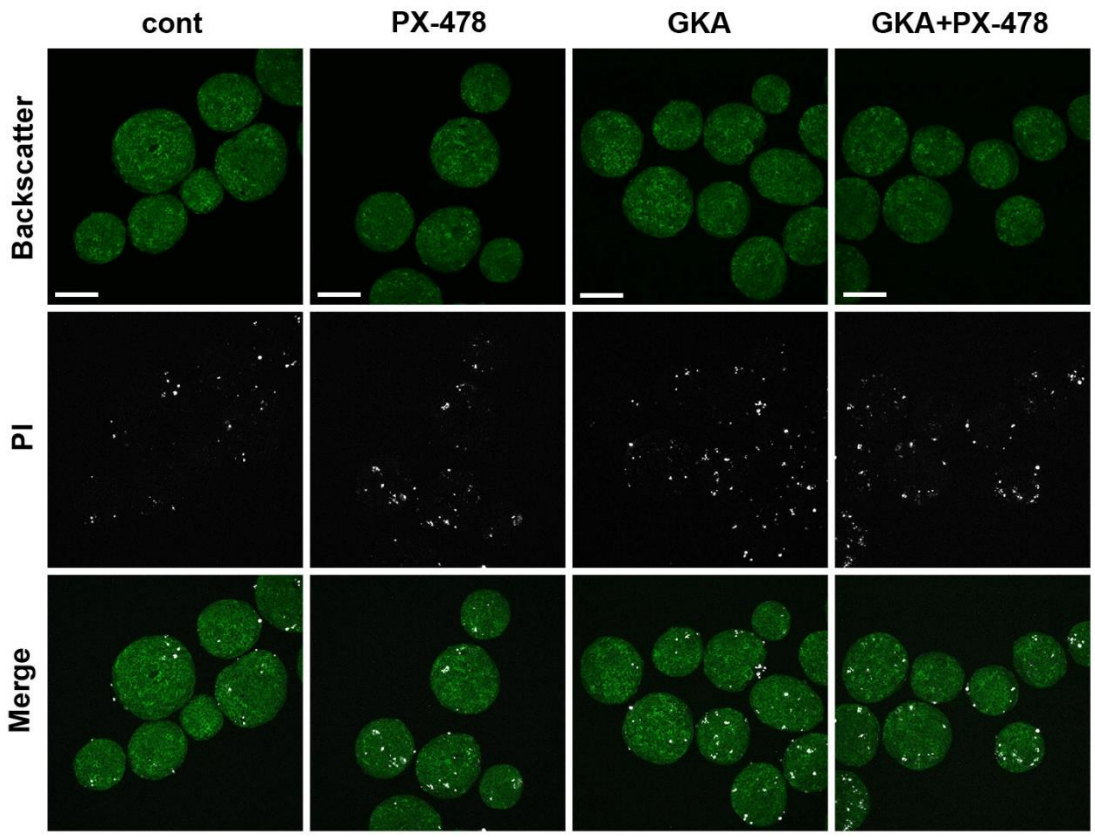

Fig. S4. Assessment of cell viability using propidium iodide. Islets from C57BL/6J mice were treated for 20 hours as indicated before incubation with propidium iodide (PI) for 10 min prior to imaging by confocal microscopy. Images are representative of n=3 experiments. Scale bars = 100 µm.

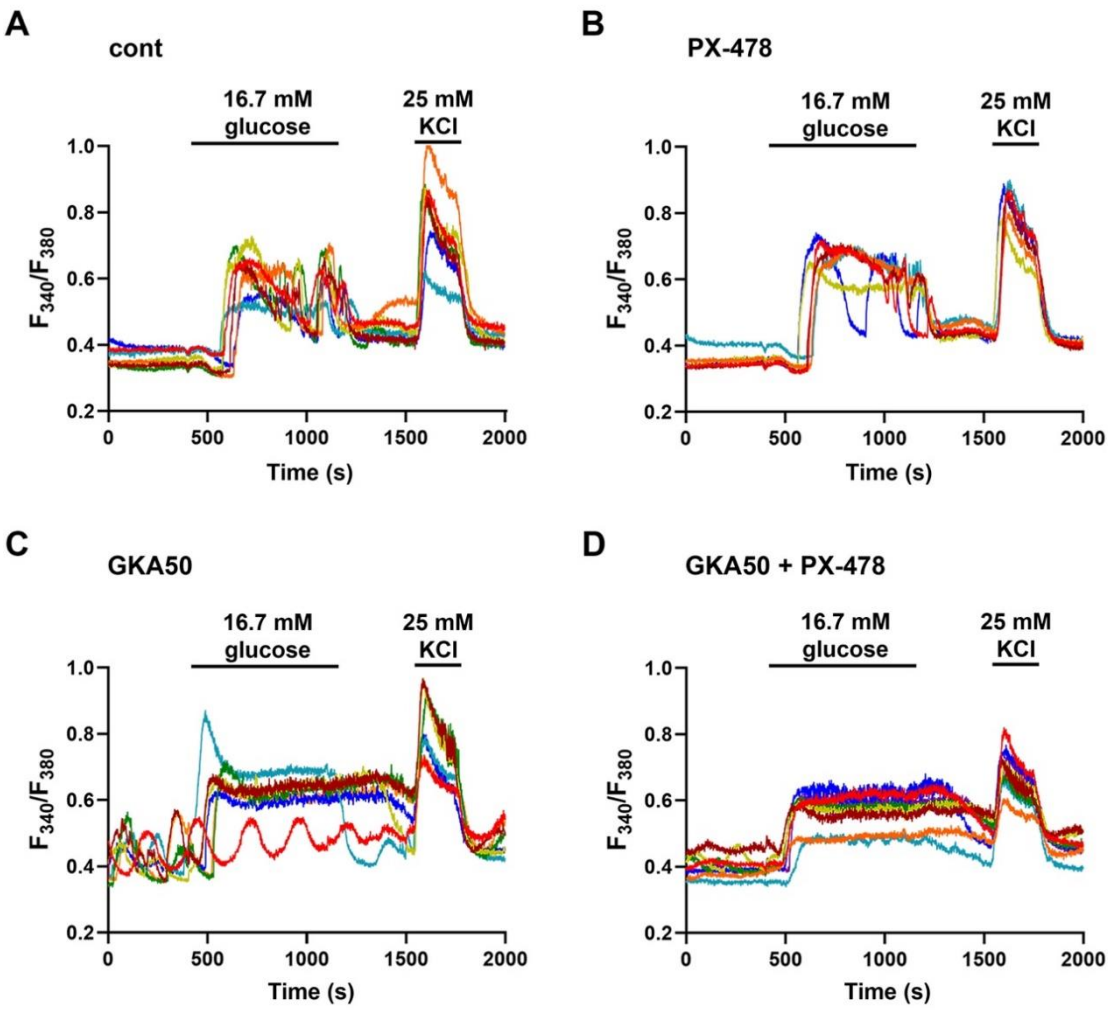

Fig. S5. Individual Ca^{2+} traces. Isolated C57BL/6J mouse islets were untreated (**A**) or treated with either PX-478 (**B**), GKA50 (**C**), or GKA60+PX-478 (**D**). After 20 hours of treatment islets were fasted for 2 hours in 3 mM glucose and $[Ca^{2+}]_i$ changes were assessed after loading with the fluorescent $[Ca^{2+}]_i$ indicator Fura-2AM. 3-4 islet preparations were used in the study. From each islet preparation $[Ca^{2+}]_i$ traces of 2-3 islets from each culture condition were analyzed.

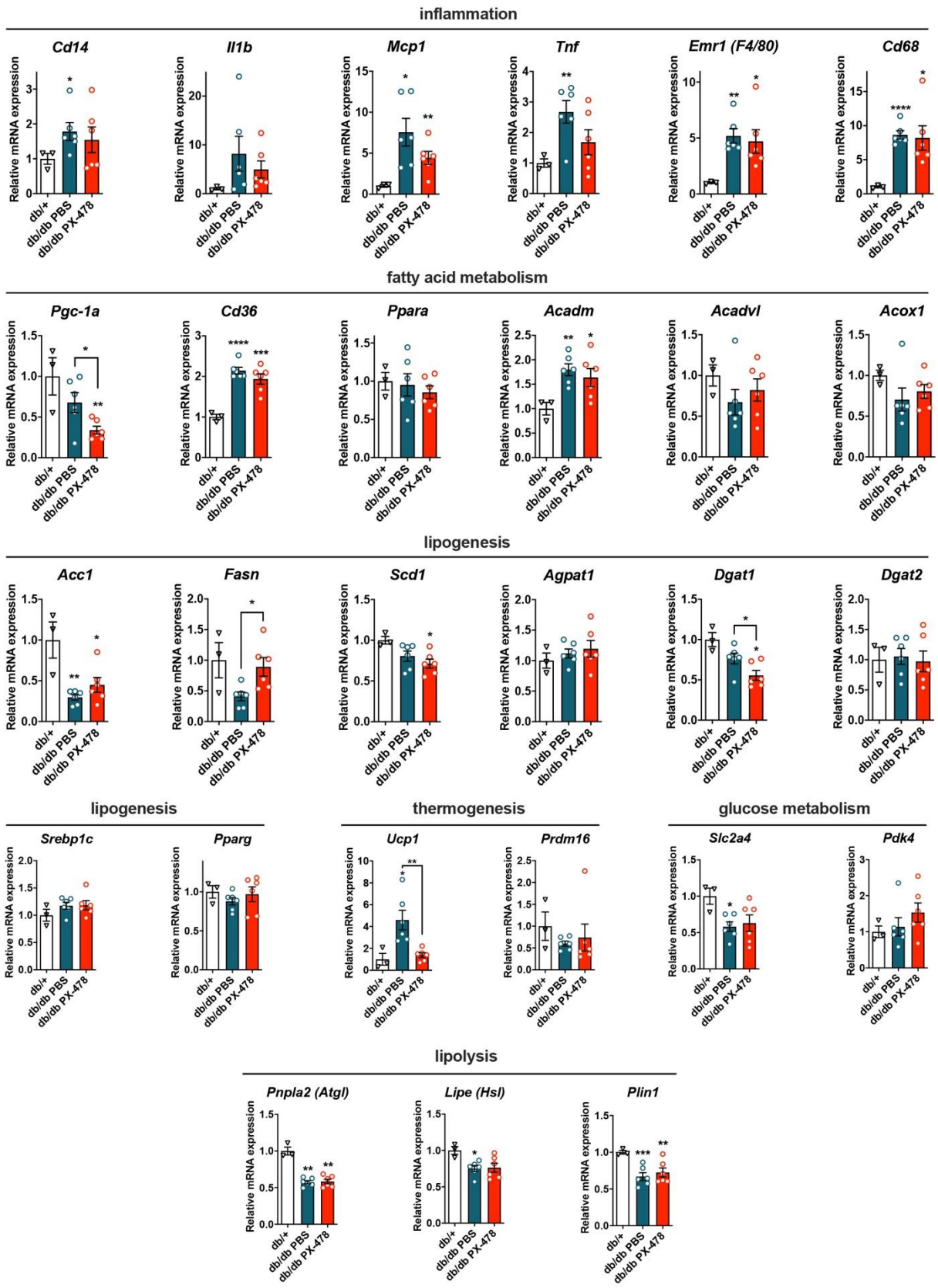
inflammation
Cd14
Il1b
Mcp1
Tnf
Emr1 (F4/80)
Cd68
fatty acid metabolism
Pgc-1a
Cd36
Ppara
Acadm
Acadvl
Acox1
lipogenesis
Acc1
Fasn
Scd1
Agpat1
Dgat1
Dgat2
lipogenesis
Srebp1c
Pparg
thermogenesis
Ucp1
Prdm16
glucose metabolism
Slc2a4
Pdk4
lipolysis
Pnpla2 (Atgl)
Lipe (Hsl)
Plin1
Relative mRNA expression
db/+
db/db PBS
db/db PX-478

Fig. S6. Treatment with PX-478 had no major impact on visceral WAT gene expression in db/db mice. As indicated in the figure, expression of genes involved in several pathways relevant for WAT function was assessed. Visceral WAT from db/db mice treated with PX-478 (n=6) or mice injected with PBS (n=6) and their lean controls db/+ (n=3) was analyzed. Expression of genes was assessed by qRT-PCR using SYBR Green. * $p<0.05$, ** $p<0.01$, *** $p<0.001$, **** $p<0.0001$ by Brown-Forsythe and Welch ANOVA tests.

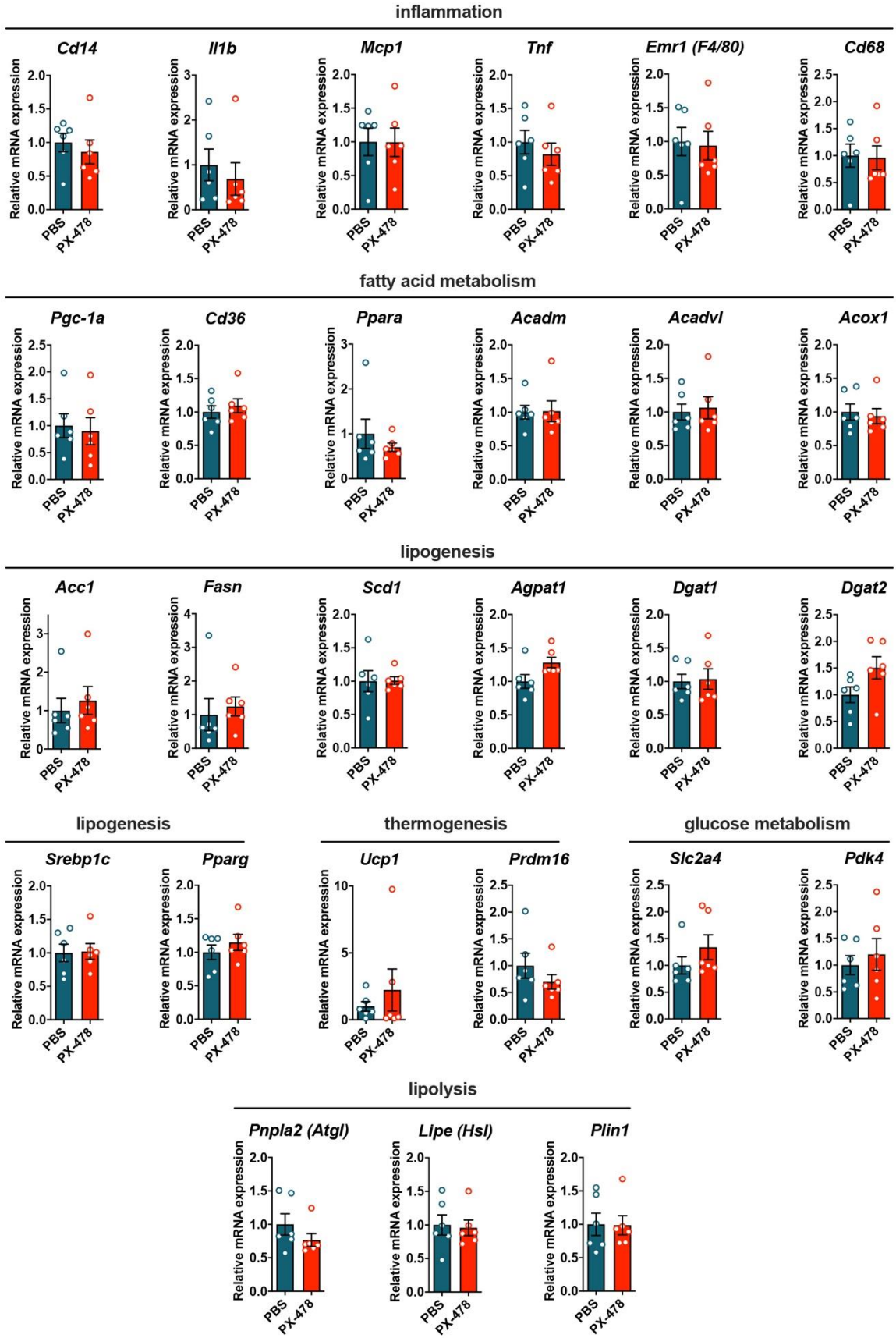
inflammation
Cd14
Il1b
Mcp1
Tnf
Emr1 (F4/80)
Cd68
fatty acid metabolism
Pgc-1a
Cd36
Ppara
Acadm
Acadvl
Acox1
lipogenesis
Acc1
Fasn
Scd1
Agpat1
Dgat1
Dgat2
lipogenesis
Srebp1c
Pparg
thermogenesis
Ucp1
Prdm16
glucose metabolism
Slc2a4
Pdk4
lipolysis
Pnpla2 (Atgl)
Lipe (Hsl)
Plin1
Relative mRNA expression
PBS
PX-478

Fig. S7. Analysis of subcutaneous WAT in treated and non-treated db/db mice show that PX-478 had no impact on gene expression. Subcutaneous WAT of db/db treated (db/db PX-478) (n=6) or non-treated (db/db PBS) (n=6) were analyzed. qRT-PCR using SYBR Green was utilized for gene expression analysis. No statistical significance was detected (two-tailed unpaired Student's t-test).

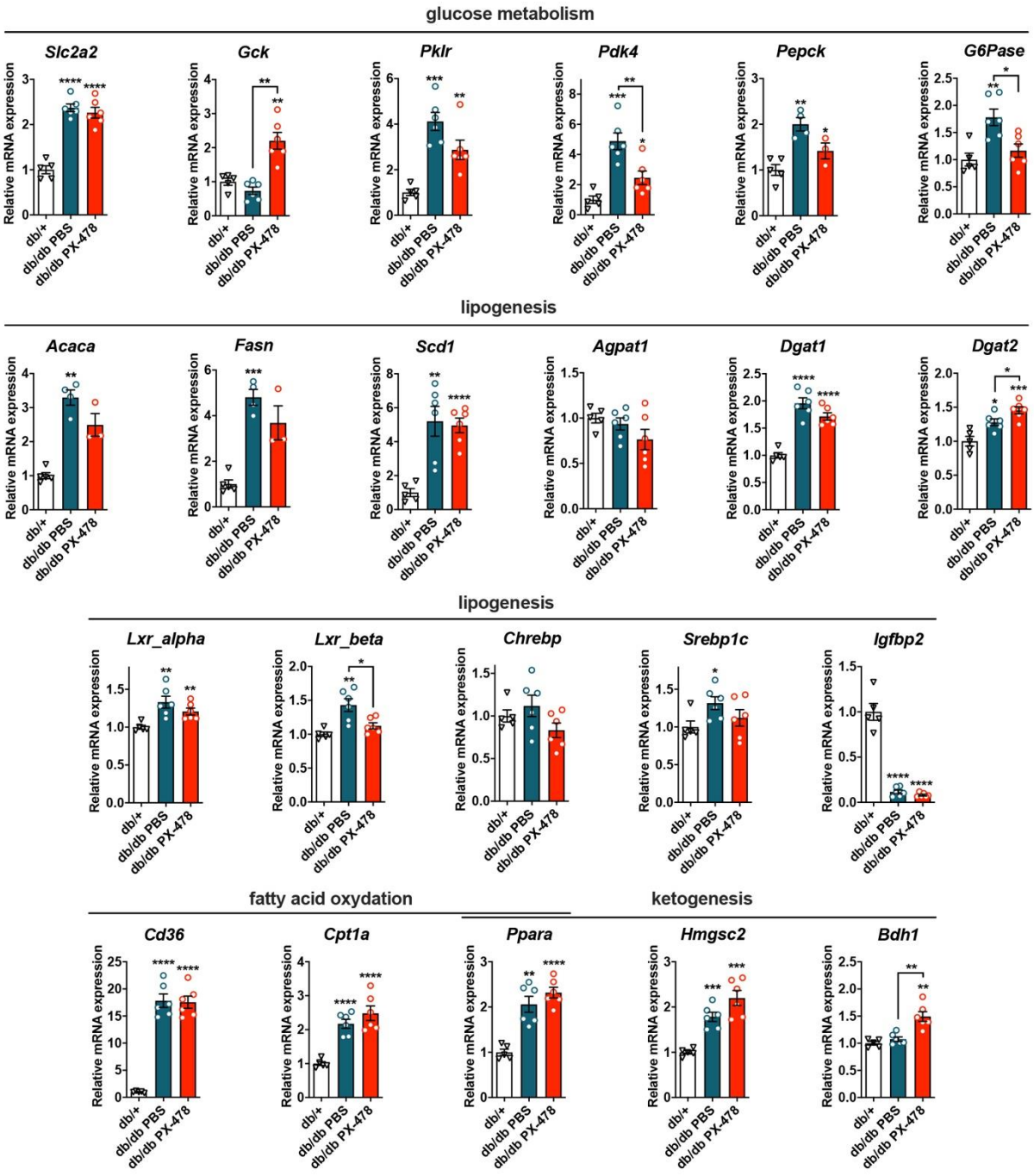

Fig. S8. Treatment with PX-478 has a positive impact on expression of genes involved in liver glucose metabolism. As indicated in the figure, several pathways relevant for liver function were investigated. Gene expression analysis of liver in PX-478 treated (n=6) and non-treated (n=6) db/db mice as well as of their lean controls db/+ (n=5) were performed by qRT-PCR. * $p<0.05$, ** $p<0.01$, *** $p<0.001$, **** $p<0.0001$ by Brown-Forsythe and Welch ANOVA tests.

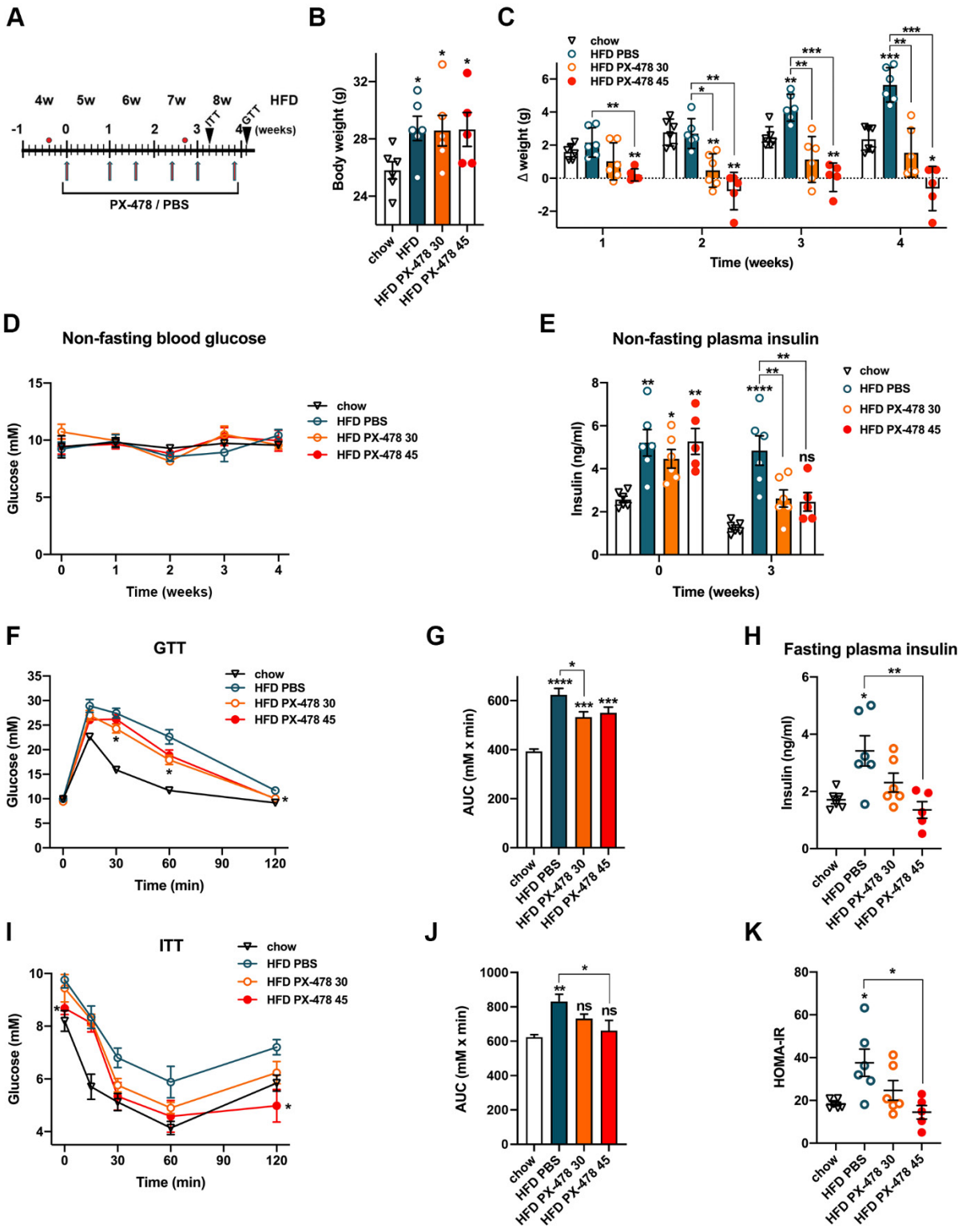

Fig. S9. Treatment of HFD-fed mice with PX-478 leads to weight loss and improvement of insulin sensitivity. (**A**) Schematic representation of the intervention strategy indicating number of

weeks of treatment with PX-478 and HFD feeding. Arrows indicate treatment days. Red dots indicate the days when blood was collected to measure non-fasting plasma insulin levels. GTT or ITT were performed at indicated days (arrowheads). (**B**) Body weight of mice at the beginning of treatment after being fed for 4 weeks with HFD. Mice were administered two distinct doses of PX-478, 30 mg/kg (HFD PX-478 30) (n=6) and 45 mg/kg (HFD PX-478 45) (n=5) or injected with PBS (HFD PBS) (n=6). Control mice were fed a chow diet (chow) (n=6). (**C**) Changes in body weight observed during 4 weeks of treatment. (**D**) Non-fasting blood glucose measured at the end of the indicated week. (**E**) After 3 weeks of PX-478 treatment a decrease in non-fasting plasma insulin is observed in treated mice when compared to HFD PBS. (**F**) GTT. Among HFD-fed mouse groups, statistically significant differences were only observed between HFD PX-478 30 and HFD PBS. (**G**) Area under the curve of GTT. (**H**) Fasting plasma insulin. (**I**) ITT. Among HFD-fed mouse groups, statistically significant differences were only observed between HFD PX-478 45 and HFD PBS. (**J**) Area under the curve of the ITT. (**K**) HOMA-IR. (F to K) Mice were fasted for 6 hours. * $p<0.05$, ** $p<0.01$, *** $p<0.001$, **** $p<0.0001$ by one-way ANOVA with Fisher's (B) or Tukey's multiple comparisons test (G, H, J and K), by two-way ANOVA with Tukey's (C, D, and E) or Fisher's multiple comparisons test (F and I). Statistical significances displayed in (F) and (I) indicate differences between HFD-fed treated and non-treated groups.

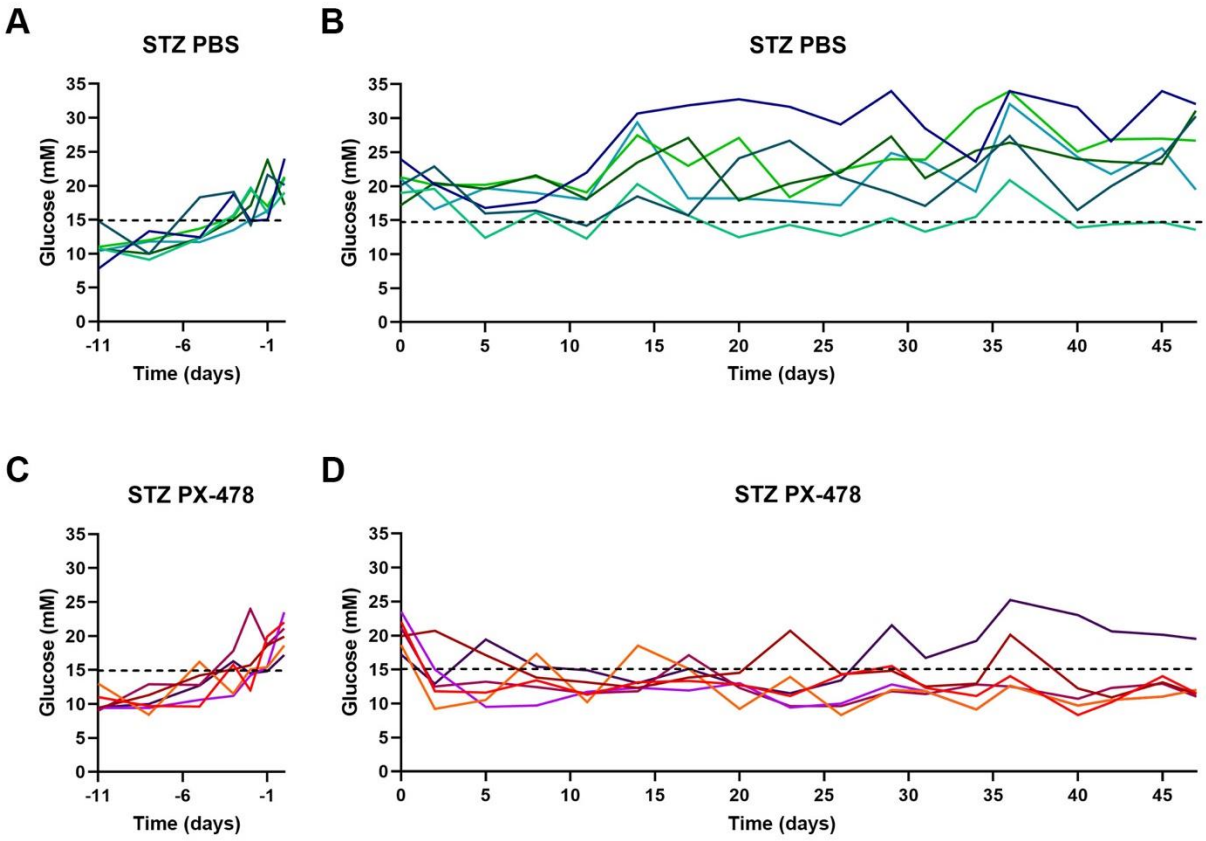

Fig. S10. Individual blood glucose concentrations of STZ-treated mice improve after PX-478 administration. (**A**) and (**C**) Blood glucose concentrations measured at different days before initiation of PX-478 treatment. The values shown for day -11 correspond to values of glycemia measured in the first day following last STZ administration. (**B**) and (**D**) Blood glucose concentrations assessed two days after each IP injection of PX-478.

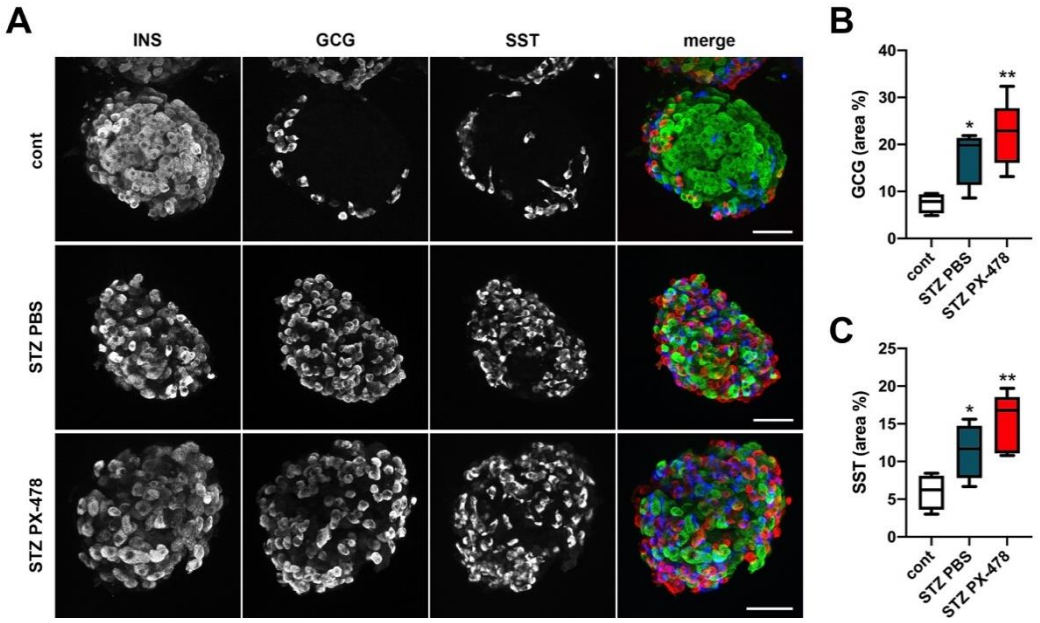

Fig. S11. PX-478 administration in STZ-treated mice does not lead to further changes in intra-islet architecture or endocrine cell content. (**A**) Whole mount immunostainings. Islets isolated from control, STZ PBS, and STZ PX-478 were stained using antibodies labeling insulin (INS, green), glucagon (GCG, red), and somatostatin (SST, blue), and imaged by confocal microscopy. No apparent differences in the architectural arrangement of these two endocrine cell types were observed between STZ PBS and STZ PX-478, showing an intermingling within the islet volume, in contrast to their mostly peripheral location in control mouse islets. (**B** and **C**) An increased number of α and ∂ cells was observed in both STZ PBS and STZ PX-478 compared to control. Analyses of (B) α cell and (C) ∂ cell areas were performed on optical imaging sections and normalized to islet areas. Confocal images are representative and presented as maximum intensity projections. Data in (B) and (C) represent average value per mouse, n=4-5 mice per group, n=6-9 islets per mouse. Scale bars = 50 μm. * $p<0.05$, ** $p<0.01$ by one-way ANOVA with Tukey's multiple comparisons test.

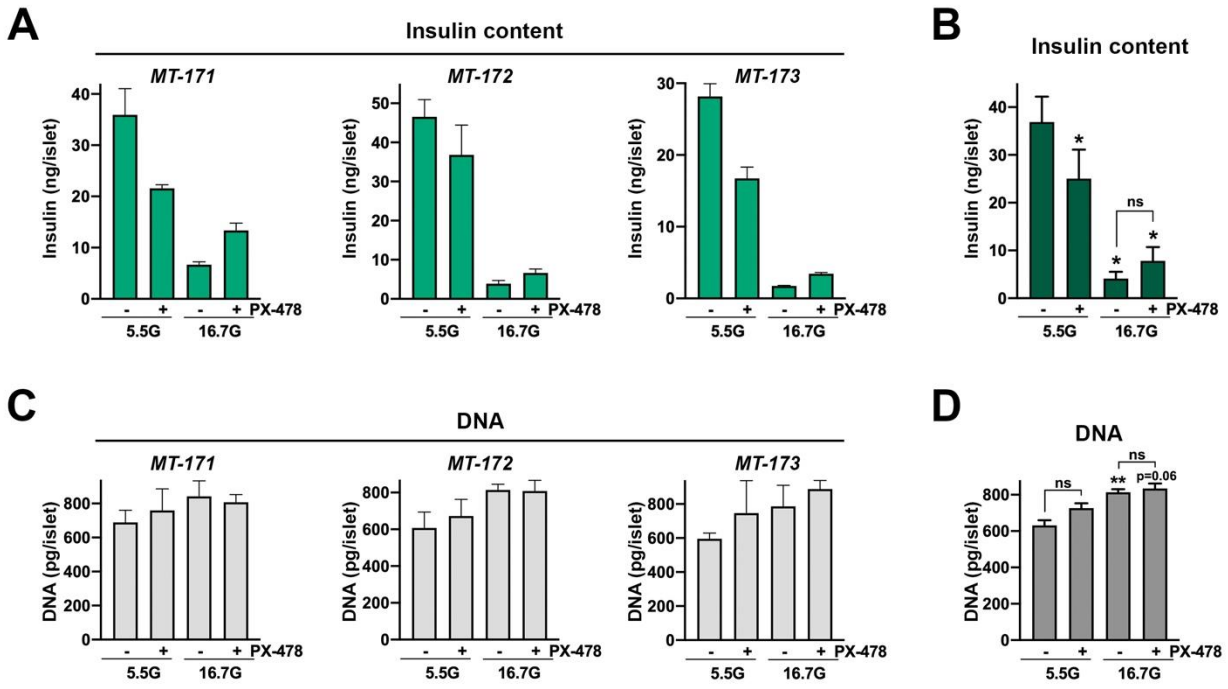

Fig. S12. Treatment with PX-478 has no impact on insulin or DNA content of human islet organoids cultured at normal or high glucose. (**A** and **C**) Insulin and DNA content of human islet organoids prepared from islets of the individual donors (MT-171, MT-172 and MT-173) after 15 days of culture in the presence of 5.5 mM (5.5G) or 16.7 mM (16.7G) glucose and treated (+) or untreated (-) with 25 μM PX-478. (**B** and **D**) Average of the three individual experiments. * $p<0.05$, ** $p<0.01$ by RM one-way ANOVA with Fisher's multiple comparisons test.

Supplementary Tables

Gene	Primer sequences
Acadm	5'- GAA GCC ACG AAG TAT GCC CT -3' 5'- CCT TCA TCG CCA TTT CTG CG -3'
Acadvl	5'- TCT TTT CCT CGG AGC ATG ACA -3' 5'- GAC CTC TCT ACT CAC TTC TCC AG -3'
Acc1 = Acaca	5'- GAT GAA CCA TCT CCG TTG GC -3' 5'- CCC AAT TAT GAA TCG GGA GTG C -3'
Acox1	5'- TGA GCT TCA TGC CCT CAC AG -3' 5'- TGC TGT GAG AAT AGC CGT GC -3'
Agpat1	5'- GAC AGA GAT ACA GCC AGC CG -3' 5'- CCA CAG CTC CAT TCT GGT CA -3'
Aldh1a3	5'- GGG TCA CAC TGG AGC TAG GA -3' 5'- CTG GCC TCT TCT TGG CGA A -3'
Ascl1	5'- GAC TTT GGA AGC AGG ATG GCA -3' 5'- CAC CCC TGT TTG CTG AGA AC -3'
Atgl = Pnpla2	5'- CTG AGA ATC ACC ATT CCC ACA TC -3' 5'- CAC AGC ATG TAA GGG GGA GA -3'
Bax	5'- AGC AAA CTG GTG CTC AAG GC -3' 5'- CCA CAA AGA TGG TCA CTG TC -3'
Bcl2	5'- GTG GTG GAG GAA CTC TTC AG -3' 5'- GTT CCA CAA AGG CAT CCC AG -3'
Bdh1	5'- ATA GGG CCT GAG AGG GAA GG -3' 5'- GCA GTA CAA ATG CAT CCC GC -3'
Bnip3	5'- ACA CCA CAA GAT ACC AAC AG -3' 5'- GAC TTG ACC AAT CCC ATA TCC -3'
Ccna2	5'- GCC TTC ACC ATT CAT GTG GAT -3' 5'- TTG CTG CGG GTA AAG AGA CAG -3'
Ccnb1	5'- GCG TGT GCC TGT GAC AGT TA -3' 5'- CCT AGC GTT TTT GCT TCC CTT -3'
Ccnb2	5'- AGC TCC CAA GGA TCG TCC TC -3' 5'- TGT CCT CGT TAT CTA TGT CCT CG -3'
Ccnd1	5'- TCC CAG ACG TTC AGA ACC -3' 5'- AGG GCA TCT GTA AAT ACA CT -3'
Cd14	5'- CTC TGT CCT TAA AGC GGC TTA C -3' 5'- GTT GCG GAG GTT CAA GAT GTT -3'
Cd36	5'- GGT GGA TGG TTT CCT AGC CTT -3' 5'- TCT ACG TGG CCC GGT TCT A -3'
CD68	5'- TGT CTG ATC TTG CTA GGA CCG -3' 5'- GAG AGT AAC GGC CTT TTT GTG A -3'
Chrebp	5'- GGG TAA TTA CTG GAA GCG GCG CAT -3' 5'- TGG ACT TAC GGA GCC GCT TTT TG -3'

Cpt1a	5’- CAC TGC AGC TCG CAC ATT AC -3’ 5’- CCA GCA CAA AGT TGC AGG AC -3’
Dgat1	5’- GCC TTA CTG GTT GAG TCT ATC AC -3’ 5’- GCA CCA CAG GTT GAC ATC C -3’
Dgat2	5’- GCG CTA CTT CCG AGA CTA CTT -3’ 5’- GGG CCT TAT GCC AGG AAA CT -3’
Emr1 (F4/80) = Adgre1	5’- TCA CTG TCT GCT CAA CCG TC -3’ 5’- AGA AGT CTG GGA ATG GGA GC -3’
Fasn	5’- AGA GAT CCC GAG ACG CTT CT -3’ 5’- GCT TGG TCC TTT GAA GTC GAA GA -3’
G6Pase	5’- CGA CTC GCT ATC TCC AAG TGA -3’ 5’- GTT GAA CCA GTC TCC GAC CA -3’
Gcg	5’- CCG CCG TGC CCA AGA TTT TGT -3’ 5’- CAC TGG TAA AGG TCC CTT CAG C -3’
Gck	5’- CAA CTG GAC CAA GGG CTT CAA -3’ 5’- TGT GGC CAC CGT GTC ATT C -3’
Glp1r	5’- GGG TCT CTG GCT ACA TAA GGA CAA C -3’ 5’- AAG GAT GGC TGA AGC GAT GAC -3’
Hk2	5’- TGA TCG CCT GCT TAT TCA CGG -3’ 5’- AAC CGC CTA GAA ATC TCC AGA -3’
Hmgsc2	5’- CCG GTG TCC CGT CTA ATG G -3’ 5’- GCA GAT GCT GTT TGG GTA GC -3’
Hsl = Lipe	5’- TCC TCA GAG ACC TCC GAC TG -3’ 5’- ACA CAC TCC TGC GCA TAG AC -3’
Iapp	5’- CTC AGA TGG ACA AAC GGA AGT G -3’ 5’- AAG TTT GCC AGG CGT TGT GT -3’
Igfbp2	5’ - CAG ACG CTA CGC TGC TAT CC -3’ 5’ - CCC TCA GAG TGG TCG TCA TCA -3’
Igfbp3	5’ - CCA GGA AAC ATC AGT GAG TCC -3’ 5’ - GGA TGG AAC TTG GAA TCG GTC A -3’
Il1b	5’- GAA ATG CCA CCT TTT GAC AGT G -3’ 5’- TGG ATG CTC TCA TCA GGA CAG -3’
Ins1	5’- TAG TGA CCA GCT ATA ATC AGA G -3’ 5’- ACG CCA AGG TCT GAA GGT CC -3’
Ins2	5’- TCT ACA CAC CCA TGT CCC GC -3’ 5’- ACA ATG CCA CGC TTC TGC TG -3’
Ki67	5’- TTG ACC GCT CCT TTA GGT ATG AA -3’ 5’- TTC CAA GGG ACT TTC CTG GA -3’
Ldha	5’- AGG CTC CCC AGA ACA AGA TT -3’ 5’- TCT CGC CCT TGA GTT TGT CT -3’
Lxr_alpha	5’- CTC AAT GCC TGA TGT TTC TCC T -3’ 5’- TCC AAC CCT ATC CCT AAA GCA A -3’
Lxr_beta	5’- ATG TCT TCC CCC ACA AGT TCT -3’ 5’- GAC CAC GAT GTA GGC AGA GC -3’
Mafa	5’- CAG CAG CGG CAC ATT CTG -3’ 5’- GCC CGC CAA CTT CTC GTA T -3’

Mcp1 = Ccl2	5’- TTA AAA ACC TGG ATC GGA ACC AA -3’ 5’- GCA TTA GCT TCA GAT TTA CGG GT -3’
Neurod1	5’- AAC AAC AGG AAG TGG -3’ 5’- TTT CTT GTC TGC CTC -3’
Nkx6.1	5’- CTC TAC TTT AGC CCC AGC G -3’ 5’- CAC GGC GGA CTC TGC ATC ACT C -3’
Pai1	5’- GAC ACC CTC AGC ATG TTC ATC -3’ 5’- AGG GTT GCA CTA AAC ATG TCA G -3’
Pbgd	5’- TCC CTG TTC AGC AAG AAG A -3’ 5’- GGC AGT GAT TCC AAC CAG -3’
Pdk1	5’- AGT CCG TTG TCC TTA TGA G -3’ 5’- CAG AAC ATC CTT GCC CAG -3’
Pdk4	5’- AGG GAG GTC GAG CTG TTC TC -3’ 5’- GGA GTG TTC ACT AAG CGG TCA -3’
Pdx1	5’- CTT AAC CTA GGC GTC GCA CAA -3’ 5’- GAA GCT CAG GGC TGT TTT TCC -3’
Pepck	5’- CTG CAT AAC GGT CTG GAC TTC -3’ 5’- CAG CAA CTG CCC GTA CTC C -3’
Pgc-1a = Ppargc1a	5’- TGA TGT GAA TGA CTT GGA TAC AGA CA -3’ 5’- GCT CAT TGT TGT ACT GGT TGG ATA TG -3’
Pgk1	5’- TCG TGA TGA GGG TGG ACT TCA ACG T -3’ 5’- GAC TGG GCT CCA TTG TCC AAG CAG -3’
Pklr	5’- TCA AGG CAG GGA TGA ACA TTG – 3’ 5’- CAC GGG TCT GTA GCT GAG TG – 3’
Plin1	5’- CAA GCA CCT CTG ACA AGG TTC -3’ 5’- GTT GGC GGC ATA TTC TGC TG -3’
Ppara	5’- CCT GAA CAT CGA GTG TCG AA -3’ 5’- ACG GCA GTA CTG GCA TTT GT -3’
Pparg	5’- GGA AGA CCA CTC GCA TTC CTT -3’ 5’- TCG CAC TTT GGT ATT CTT GGA G -3’
Ppy	5’- AAT GTA CCC AGG CGA CTA TG -3’ 5’- GTT CTC CTC CTC GGC TCT CTT C -3’
Prdm16	5’- CAG CAC GGT GAA GCC ATT C -3’ 5’- GCG TGC ATC CGC TTG TG -3’
Scd1	5’- GGG CAG TTC TGA GGT GAT TAG -3’ 5’- TTC ATG GCA GTG GGT AGG TAG -3’
Serpina7	5’- TCC CCT GTG AGC ATA TCT GTT -3’ 5’- CGG GAG TAT CTG TGA GGT TAA AC -3’
Slc2a1 = Glut1	5’- TGT ATC CTG TTG CCC TTC TG -3’ 5’- CTT CTT CAG CAC ACT CTT GG -3’
Slc2a2 = Glut2	5’- ATT CTT TGG TGG GTG GCT CG -3’ 5’- CAG CAA TGA TGA GGG CGT GT -3’
Slc2a4 = Glut4	5’- GTG ACT GGA ACA CTG GTC CTA -3’ 5’- CCA GCC ACG TTG CAT TGT AG -3’

Slc30a8	5'- CAG AGA ACT TCG ACA GAA GCC -3' 5'- CTT GCT TGC TCG ACC TGT T -3'
Srebp1c = Srebf1	5'- GAT GTG CGA ACT GGA CAC AG -3' 5'- GCA TGT CTT CGA TGT CGT TCA AA -3'
Sst	5'- TCC TGG CTT TGG GCG GTG TC -3' 5'- CCA GCC TCA TCT CGT CCT GC -3'
Tnf	5'- CAG GCG GTG CCT ATG TCT C -3' 5'- CGA TCA CCC CGA AGT TCA GTA G -3'
Tnfrsf10b	5'- TTG ACT ACA CCA GCC ATT CCA A -3' 5'- CGT CAG TGC AGT TAG AGC -3'
Trpm5	5' - TGC TCA AGG GTA CCC AAT GCT ACT -3' 5'- CCG GGT GTT TGA AAT GTC CCG TTT -3'
Ucn3	5'- GCT GTG CCC CTC GAC CT -3' 5'- TGG GCA TCA GCA TCG CT -3'
Ucp1	5'- CAA TGA ACA CTG CCA CAC CTC -3' 5'- GGC ATT CAG AGG CAA ATC AGC T -3'

Table S1. Primers used for qRT-PCR experiments.

Organoid #	**UNOS ID#**	**Age**	**Gender**	**Ethnicity**	**BMI**	**HbA1c**
MT-171	AIBE224	48	Male	Asian	22.3	5.2 %
MT-172	AIEY035	19	Male	Caucasian	23.2	5.8 %
MT-173	AIFA337	18	Male	Hispanic	20.5	5.9 %

Table S2. Human donor profiles corresponding to individual organoid production lots.

Organoid #	**Diameter**	**IEQ/organoid**	**ATP content**	**Stimulation index**
MT-171	161 ± 9 µm	1.26 ± 0.21	2.8 ± 0.3 pmol/IEQ	7
MT-172	160 ± 7 µm	1.27 ± 0.14	3.1 ± 0.2 pmol/IEQ	16
MT-173	153 ± 8 µm	1.08 ± 0.17	3.0 ± 0.3 pmol/IEQ	10

Table S3. Morphological and functional characterization of human islet organoid production lots. IEQ = islet equivalent. Insulin secretion was measured at 2.8 mM and 16.7 mM glucose to determine stimulation index. Characterizations were performed prior to transportation (see Supplementary Materials and Methods section).